Ehrlichia SLiM ligand mimetic activates Hedgehog signaling to engage a BCL-2 anti-apoptotic cellular program

Caitlan D. Byerly[1], Shubhajit Mitra[1], LaNisha L. Patterson[1], Nicholas A. Pittner[1], Thangam S. Velayutham[1], Slobodan Paessler[1,6], Veljko Veljkovic[6], and Jere W. McBride[1-5 #]

Departments of Pathology[1] and Microbiology and Immunology,[2]

Center for Biodefense and Emerging Infectious Diseases,[3]

Sealy Institute for Vaccine Sciences[4] and

Institute for Human Infections and Immunity[5]

University of Texas Medical Branch, Galveston, Texas, USA

Biomed Protection, LLC, Galveston, Texas, USA[6]

Running Title: *Ehrlichia* SLiM activation of Hedgehog signaling

Corresponding author:

Jere W. McBride, Ph.D.
Department of Pathology
University of Texas Medical Branch
Galveston, TX 77555-0609
Tel: (409) 747-2498
Email: jemcbrid@utmb.edu

Abstract

Ehrlichia chaffeensis (*E. chaffeensis*) has evolved eukaryotic ligand mimicry to repurposes multiple cellular signaling pathways for immune evasion. In this investigation, we demonstrate that TRP120 has a novel repetitive short liner motif (SLiM) that activates the evolutionarily conserved Hedgehog (Hh) signaling pathway to inhibit apoptosis. *In silico* analysis revealed that TRP120 has sequence and functional similarity with Hh ligands and a candidate Hh ligand SLiM was identified. siRNA knockdown of Hh signaling and transcriptional components significantly reduced infection. Co-immunoprecipitation and surface plasmon resonance demonstrated that rTRP120-TR interacted directly with Hh receptor Patched-2 (PTCH2). *E. chaffeensis* infection resulted in early activation of Hh transcription factor GLI-1 and upregulation of Hh target genes. Moreover, soluble recombinant TRP120 (rTRP120) activated Hh and induced gene expression consistent with the eukaryotic Hh ligand. The TRP120 Hh SLiM (NPEVLIKD) induced nuclear translocation of GLI-1 in THP-1 cells and primary human monocytes and induced a rapid and expansive activation of Hh pathway target genes. Furthermore, Hh activation was blocked by an α-TRP120 Hh SLiM antibody. TRP120 Hh SLiM significantly increased levels of Hh target, anti-apoptotic protein B-cell lymphoma 2 (BCL-2), and siRNA knockdown of BCL-2 dramatically inhibited infection. Blocking Hh signaling with the inhibitor Vismodegib, induced a pro-apoptotic cellular program defined by decreased mitochondria membrane potential, significant reductions in BCL-2, activation of caspase 3 and 9, and increased apoptotic cells. This study reveals a novel *E. chaffeensis* SLiM ligand mimetic that activates Hh signaling to maintain *E. chaffeensis* infection by engaging a BCL-2 anti-apoptotic cellular program.

Author summary

Ehrlichia chaffeensis is an obligately intracellular bacterium that preferentially infects and replicates within mononuclear phagocytes and survives intracellularly by modulating cellular signaling pathways to subvert innate immune defenses. This investigation reveals the complex and expanding role that the *E. chaffeensis* TRP120 moonlighting effector and SLiM ligand mimetics have on immune subversion and infection through activation and regulation of evolutionarily conserved signaling pathways. Herein, we define a TRP120 Hh SLiM mimetic that induces Hh signaling and regulates the anti-apoptotic protein BCL-2 to prevent sequential activation of caspase 9 and 3, promoting *E. chaffeensis* infection. This study defines a novel prokaryotic SLiM mimetic that repurposes evolutionarily conserved eukaryotic signaling pathways to promote survival of an intracellular bacterium.

Introduction

Ehrlichia chaffeensis (*E. chaffeensis*) is an obligately intracellular tick-borne rickettsial pathogen and the etiologic agent of human monocytotropic ehrlichiosis (HME), an emerging, life-threatening zoonosis. Mononuclear phagocytes are preferentially infected by *E. chaffeensis,* where it replicates in early endosome-like host membrane-derived cytoplasmic vacuoles and completes a biphasic intracellular life cycle (1). During infection, *E. chaffeensis* secretes well characterized tandem repeat protein (TRP) effectors via the type 1 secretion system (T1SS) which interact with a diverse array of host proteins (2). TRP-host interactions rewire fundamental host cell processes such as gene transcription and activation of conserved cellular signaling pathways (Wnt and Notch), through interactions that involve post-translational modifications and SLiM mimicry in order to reprogram the host cell and subvert innate immune defenses (3-9).

Ehrlichia chaffeensis TRP120 has been recognized as a moonlighting protein that has multiple roles during infection (10). Initially, TRP120 was identified as a major immunoreactive protein, but was later detected in the nucleus where it functions as a nucleomodulin. Subsequently, yeast-2-hybrid (Y2H) studies identified a multitude of molecular interactions between TRP120 and eukaryotic proteins involved in various cellular processes, including cell signaling, transcriptional regulation, PTMs and apoptosis (3). Recently, multiple TRP120 functions that have been well defined including DNA binding (11), HECT E3 ubiquitin ligase activity (6, 8, 12), and ligand mimicry (7). Notably, TRP120 engages Notch and Wnt receptors to activate conserved Notch and Wnt signaling through SLiM ligand mimicry (7, 9). SLiM ligand mimicry and

post translational modification (PTM) SLiMs have been well characterized in bacteria and viruses (7, 13, 14). However, examples of interkingdom Hedgehog (Hh) SLiM mimicry have never been reported.

The Hh pathway is an evolutionarily conserved signaling pathway that plays a crucial role in embryogenesis (15). The pathway was first identified in *Drosophila* and extensively studied in the field of developmental biology for its role in segment polarity and body patterning during embryogenesis (16). Hh signaling components are highly conserved in vertebrates and invertebrates, but the key difference is in pathway redundancy (17). In *Drosophila* there is one ligand (Hh), one primary receptor (PTC) and one transcription factor (Ci). However, in mammals the Hh pathway has three families of ligands: Sonic hedgehog (Shh); Indian hedgehog (Ihh) and Desert hedgehog (Dhh) two primary receptors (PTCH1 and PTCH2) and three transcription factors (GLI-1, GLI-2, and GLI-3). (18, 19). Hh signaling is initiated by the Hh ligand binding to the Hh receptor Patched (PTCH). This interaction counters PTCH-mediated repression of Smoothened (SMO) and activates the only known transcriptional mediators, the GLI family of Hh transcription factors (20). Regardless, the signal is relayed from external milieu to nucleus in a moderately conserved way (16). In humans, the Hh pathway is involved in maintaining tissue homeostasis, and aberrant activation of this pathway results in the formation of various tumors and hematological malignancies (21, 22). Hh has also been identified as a key regulator in maintaining tissue homeostasis and remodeling due to various roles associated with cell proliferation, angiogenesis, B and T cell development, regulation of immune response, autophagy and cellular apoptosis

(23). Notably, evolutionary conserved signaling pathways such as Hh are known to be engaged by pathogens. Viral and bacterial pathogens including Hepatitis B and C (HBV and HCV, respectively), Epstein–Barr virus (EBV), Influenza A virus, *Helicobacter pylori,* and *Mycobacterium bovis* have recently been reported to modulate Hh signaling during infection (19). As cellular apoptosis is highly regulated by Hh (24), exploiting the Hh pathway may be an important strategy for intracellular pathogens to enhance host cell survival to promote intracellular infection (25).

Apoptosis is the default programmed cell death mode for organ development during embryogenesis and has emerged as one of the major pathways controlled by Hh signaling (23, 26). Moreover, apoptosis also plays an important role in host immune defense during microbial infections, triggering the sequential activation of caspases, in response to either an extrinsic or intrinsic death signal (27). The release of cytochrome c from the mitochondria initiates the intrinsic apoptotic pathway and results in cytochrome c association with apoptotic protease activating factor 1 (Apaf-1) and procaspase 9 to form the apoptosome, a multimeric protein complex involved in cleavage of inactive caspase 9 into the active form (28). Caspase 9 cleaves procaspase 3, to form active caspase 3, which is essential for chromatin condensation and DNA fragmentation in all apoptotic cells (29). One of the major anti-apoptotic transcriptional targets of GLI-1 is BCL-2, which is essential in inhibiting apoptosis inducer Bax (30, 31). The anti-apoptotic members of the BCL-2 family maintain mitochondrial membrane integrity by sequestering BH3-only proteins like Bax and Bak to inhibit the release of cytochrome c from mitochondria, thereby inhibiting apoptosis (32). Moreover, *E.*

105 *chaffeensis* influences the transcriptional activity of other Hh-targeted anti-apoptotic
106 genes such as *BCL2A*, *MCL1*, and *BIRC3* (8, 33, 34).
107
108 This investigation reveals a novel host-pathogen strategy, whereby *E. chaffeensis*
109 utilizes eukaryotic SLiM mimicry to exploit Hh signaling to activate an anti-apoptotic
110 cellular program. We determined that *E. chaffeensis* TRP120 directly interacts with Hh
111 receptor, PTCH2 and Hh signaling is activated through a Hh ligand SLiM mimetic.
112 Furthermore, we analyzed the role of Hh signaling in regulating apoptosis during
113 infection and demonstrate that *E. chaffeensis* exploits Hh signaling to engage BCL-2
114 and inhibit apoptosis during infection.
115
116 **Results**
117 ***E. chaffeensis* TRP120 contains a predicted Hh ligand SLiM.**
118 TRP120 contains a tandem repeat domain (TRD) centered between the N- and C-
119 terminal domains. Various functional SLiMs have been reported within the N terminus,
120 TRD, and C terminus that are relevant to *E. chaffeensis* infection, including
121 posttranslational modification motifs, DNA-binding motifs, and ubiquitin ligase catalytic
122 motifs (7). We previously reported that TRP120 stimulation results in transcriptional
123 upregulation of *GLI-1* in THP-1 cells (4). Moreover, during *E. chaffeensis* infection Wnt
124 and Notch signaling pathways are activated through ligand mimicry via TRP120 Wnt
125 and Notch SLiMs (4, 7, 9, 10). Since GLI-1 is a major transcriptional factor of the Hh-
126 signaling pathway and often cross-talks with Wnt and Notch signaling (35, 36), we
127 investigated the possibility of Hh pathway activation during *E. chaffeensis* infection.

Using NCBI Protein BLAST and ISM analysis, we determined that TRP120 has sequence homology and functional similarity with Hh ligands respectively within the TRD **(Fig. 1)**. Specifically, the homologous TRP120 Hh sequence (NPEVLIKD) present in each TR is 87% similar to the Hh ligand sequence that is associated with the Hh-PTCH binding site (37). In addition, the homologous TRP120 Hh sequence is 8 aa, consistent in length with other known SLiMs **(Fig. 1A)**. Therefore, the homologous TRP120 Hh sequence was designated as the TRP120 Hh SLiM.

While sequence homology can be a useful tool to determine whether a bacterial protein may mimic a eukaryotic motif, amino acid sequence homology does not suggest functional similarity. To predict functional similarity between TRP120 and Hh ligands, we performed an information spectrum method (ISM) analysis comparing TRP120 to Dhh and Ihh **(Fig. 1B-D)**. ISM analysis is performed *in silico* to identify shared characteristics between two molecules by predicting similar long-wave frequency vibrations that dictate various protein functions (38). TRP120-Dhh **(Fig. 1B)** and TRP120-Ihh **(Fig. 1C)** ISM cross-spectrum electron-ion interaction potentials (EEIP) detected significant peak amplitude at frequency 0.457, indicating a shared biological function between TRP120 with Dhh and Ihh in the same region. Scanning the EEIP sequence of TRP120 along the peak amplitude frequency identified the amino acids contributing to shared biological function between TRP120 with Dhh and Ihh. The shared biological function resides in the TRD of TRP120, immediately upstream of the predicted TRP120 Hh SLiM **(Fig. 1D)**. Together, the BLAST and ISM analysis results suggest that TRP120 contains

a Hh SLiM within the TRD that has sequence similarity with the receptor-binding site of Hh ligands and is predicted to have functional similarity with Hh ligands by ISM.

Hh signaling components are required for *E. chaffeensis* survival.

The Hh signaling pathway is not only required during embryogenesis, but also plays a major role in determining cell fate in adult hematopoietic cells. Since Hh signaling is involved in different cellular processes like autophagy and apoptosis (39, 40), which are crucial for ehrlichial intracellular survival (41), we examined the effect of Hh signaling inhibition on *E. chaffeensis* infection using iRNA to individually target and silence *GLI-1/2/3, PTCH1, PTCH2* and *SMO* in THP-1 cells. *E. chaffeensis* infection (depicted by *dsb* levels) was significantly reduced in nearly all transfection groups 24 post transfection of siRNA (excluding *PTCH1*-KD cells), relative to the infection level in scrambled siRNA-transfected cells **(Fig. 2A)**. The most significant impact on *E. chaffeensis* infection occurred in *GLI-1-, PTCH2-* and *SMO*-KD cells. Loss of PTCH2 receptor significantly reduced infection, while loss of PTCH1 receptor did not, suggesting that *E. chaffeensis* may preferentially target PTCH2 during infection.

TRP120 interacts with Hh receptor PTCH2.

Hh signaling initiates when a Hh ligand binds to the PTCH receptor, disengaging PTCH-mediated inhibition of SMO, which results in nuclear translocation of the full-length GLI-1 transcription factor and subsequent activation of Hh pathway target genes (17). A Hh SLiM mimetic was identified and iRNA KD studies performed suggests that *E. chaffeensis* interacts with PTCH2 for Hh activation. Based on these results, we

hypothesized that TRP120 is a Hh ligand mimic that directly interacts with PTCH2. To examine the cellular distribution and colocalization of PTCH2 with the TRP120-expressing ehrlichial inclusions, cells were stained with anti-PTCH2 and anti-TRP120 specific antibody and observed by immunofluorescence microscopy. We found a mostly punctate distribution of PTCH2 receptors in uninfected THP-1 cells; however, in infected cells, we found colocalization of PTCH2 with morulae expressing TRP120 (**Fig 3A**). Intensity correlation analysis using ImageJ demonstrated a strong Pierson's correlation coefficient (PCC=0.866) between PTCH2 and TRP120. In addition, colocalization of native PTCH2 receptor and ectopically expressed GFP-TRP120 in transfected HeLa cells supports that an interaction exists between TRP120 and PTCH2 (**Fig 3B)**. Since these data only indicate TRP120 colocalization with PTCH2, we performed two protein-interaction assays, including Co-IP and surface plasmon resonance (SPR). We confirmed the direct interaction between TRP120 and PTCH2 by immunoprecipitating TRP120 or PTCH2 (reverse Co-IP) from the lysate of infected THP-1 cells harvested at 0 hpi (uninfected control) and 24 hpi, which ensured that sufficient levels of TRP120 were present **(Fig. 3C)**. An interaction between PTCH2 and TRP120 was detected with Co-IP which was also demonstrated with reverse Co-IP. Additionally, SPR was utilized to confirm a direct interaction between TRP120 TRD and PTCH2 and determine the binding affinity **(Fig. 3D)**. A strong interaction between rPTCH2 and rTRP120-TR (K_D = 4.40 ± 1.5 nM) was detected compared to the negative control (K_D = 0). These data demonstrate that TRP120 directly interacts with PTCH2 via the TRD **(Fig. 3)**, which contains both sequence and functional similarity with Hh ligands **(Fig. 1)**. These results identified PTCH2 as a receptor for TRP120.

196

197 ***E. chaffeensis* activates the Hh signaling pathway in THP-1 cells and PHMs.**

198 Hh signal initiates at the plasma membrane when Hh ligands interacts with the 12-pass-
199 transmembrane PTCH receptor. The Hh ligand-PTCH interaction results in increased
200 expression of cell surface receptor SMO, decreased levels in the cytoplasmic negative
201 regulator SUFU, and subsequent activation and nuclear translocation of Hh transcription
202 factor, GLI-1 (42-44). We predicted an *E. chaffeensis* TRP120 Hh SLiM and identified a
203 direct interaction between TRP120 and PTCH2 during infection. Additionally, we
204 previously reported that TRP120 stimulation results in transcriptional upregulation of
205 *GLI-1* in THP-1 cells (4). However, the role of *E. chaffeensis* in activating the Hh
206 signaling pathway has not been defined. Hence, we investigated whether *E. chaffeensis*
207 activates GLI-1 in THP-1 cells and PHMs via confocal microscopy **(Fig. 4)**. We first
208 determined that *E. chaffeensis* stimulates GLI-1 activation and nuclear translocation in
209 THP-1 cells. GLI-1 was detected in the nucleus within 2 hpi, and progressive nuclear
210 accumulation of GLI-1 was observed over 48 hpi compared to uninfected controls at
211 respective timepoints (**Fig. 4A**). Further, *E. chaffeensis*-infected PHMs stimulated GLI-1
212 activation and nuclear translocation at 10 hpi compared to the uninfected control, which
213 provided further evidence that *E. chaffeensis* activates Hh signaling (**Fig 4B**).

Expression array analysis of Hh-signaling genes during *E. chaffeensis* infection.

To further examine the role of *E. chaffeensis* in Hh pathway activation, we examined Hh pathway gene transcription during *E. chaffeensis* infection. A transcriptional analysis was performed using a human Hh signaling PCR array, including Hh components, putative targets, and auxiliary genes at 4h, 8h, 24h and 48 hpi **(Fig. 5**). Volcano plots generated from data set at 4h, 8h, 24h, and 48 hpi depict a differential expression pattern of Hh signaling pathway genes in the *E. chaffeensis*-infected cells compared to uninfected cells **(Fig. 5A)**. Significant activation of Hh pathway regulator, component, and target genes was detected between 4h, 8h, 24h, and 48 hpi. Only a small number of Hh-associated genes were negatively regulated during infection. The expression patterns of genes that showed a consistent and a significant upregulation throughout all different time points included Hh pathway regulators: *BOC, CDON, BTRC, CSNK1E* and *PRKACA;* Hh signaling pathway auxiliary genes: *LATS1, MAPK1* and *NF2* and the Hh pathway target genes: *MTSS1, WNT10A, WNT3, WNT9a and VEGFA.* The core Hh signaling pathway receptor genes like *PTCH1, PTCH2 and SMO* were highly expressed during early and late time points, suggesting high pathway activity throughout *E. chaffeensis* infection. One of the major anti-apoptotic genes and a major target of Shh-signaling pathway *BCL2* showed transcriptional upregulation at 24 and 48 hpi suggesting a crucial role of Hh signaling pathway in inhibition of host cell apoptosis during *E. chaffeensis* infection. The normalized expression of selected genes in the Hh PCR array between infected and uninfected cells at 48 hpi is shown in **Fig. 5B**.

We also confirmed immunofluorescence results by immunoblot by probing nuclear fractions of uninfected and *E. chaffeensis*-infected THP-1 cells with GLI-1 specific

antibody. Progressive nuclear accumulation of GLI-1 was observed over 48 hpi (**Fig 6A**). In addition, we tested cytoplasmic fractions of SMO during *E. chaffeensis*-infection and found induced SMO protein expression during infection. In addition, we also detected decreased protein expression of cytoplasmic GLI-1 negative regulator SUFU and increased protein expression of Shh in *E. ch.*-infected THP-1 cytoplasmic fractions **(Fig. 6B)**. Collectively, these data demonstrates that *E. chaffeensis* activates the Hh-signaling pathway during infection.

TRP120 activates GLI-1 and Hh gene expression consistent with Hh ligands.

To further examine the role of TRP120 in Hh pathway activation, purified rTRP120-FL (1 µg/ml) was used to stimulate THP-1 cells and PHMs, and cellular expression and distribution of GLI-1 were monitored using confocal microscopy **(Fig. 7A-B)**. GL-1 activation, accumulation and nuclear translocation was observed in THP-1 cells **(Fig. 6A)** and PHMs **(Fig. 7B)** at 6 h and 10 hpt, respectively. THP-1 cells and PHMs treated with rTRP120-FL demonstrated clear GLI-1 activation, similarly to recombinant Shh (rShh), which was used as a positive control. To further confirm the role of TRP120 in activation of the Hh pathway, cells were stimulated with rTRP120-FL or rShh for 24 h, and transcriptional analysis was performed using a human Hh signaling PCR array **(Fig. 7C-D).** The volcano plot represents gene expression patterns of all 84 genes in Hh signaling PCR array in cells stimulated with rTRP120-FL normalized to negative control cells treated with rTrx. A significant increase in 15 Hh genes, including Hh pathway associated receptors, and cofactors (*PTCH2*, *SMO, CDON* and *LRP2*), regulators (*BTRC, CSNK1E* and *PRKACA*), transcription factor (*GLI1*), and target genes

(*WNT10A, WNT6, WNT2B* and *WNT4*) was detected **(Fig. 7C).** In addition, 2 genes (*WIF1 and GAS1*) were downregulated compared to the control **(Fig. 7C)**. In comparison, cells treated with rShh had a significant increase in 17 genes in the Hh pathway array (**Fig. 7D**). Though there were differential expression pattern of genes in TRP120 and Shh treated cells, we found 8 Hh pathway-associated genes including (*PTCH2*, *SMO, GLI1, CSNK1E, and LRP2*) and target genes (*WNT10A, WNT4, and WNT6*) were upregulated in both rTRP120-FL and rShh treatment. Together these data demonstrate that TRP120 independently and efficiently activates the Hh signaling pathway**.**

TRP120 Hh SLiM activates GLI-1 in THP-1 cells and PHMs.

We next investigated if the predicted TRP120 Hh SLiM sequence (NPEVLIKD) was sufficient in activating Hh signaling **(Fig. 8)**. A table was used to reveal various TPR120 peptide sequences within the TRP120 TRD domain. TRP120-TR-Hh (20 aa) and TRP120-Hh-SLiM (8 aa) sequences contain the TRP120 Hh homology sequence. More specifically, the TRP120-Hh-SLiM sequence is the sequence that was specifically defined through BLAST analysis. TRP120-Hh-SLiM-mut (18 aa) is a corresponding mutant peptide with guanine and adenine substitutions that replace the TRP120 Hh SLiM aa's. TRP120-TR (-) (22 aa) is a TRP120 TRD sequence that does not contain the defined Hh homology sequence **(Fig. 8A)**. THP-1 cells were treated with TRP120-TR-Hh, TRP120-TR (-), TRP120-Hh-SLiM or TRP120-Hh-SLiM-mut for 6 h, and GLI-1 signaling was measured as described. Both TRP120-TR-Hh and TRP120-Hh-SLiM treatments elicited a significant increase in GLI-1 activity, while TRP120-TR (-) and

TRP120-Hh-SLiM-mut control could not activate GLI-1 **(Fig. 8B)**. Similarly, TRP120-Hh-SLiM treatment elicited a significant increase in GLI-1 activity in PHMs at 10 hpt, but TRP120-Hh-SLiM-mut did not **(Fig. 8C)**. Additionally, THP-1 cells treated with 50 ng/mL or 500 ng/mL of TRP120-Hh-SLiM exhibited Hh gene regulation in a concentration dependent manner **(Fig. 8D-E)**. TRP120-Hh-SLiM significantly activated Hh target genes at 24 hpt compared to untreated **(Fig. 8D)** and TRP120-Hh-SLiM-mut treated **(Fig. 8E)** cells, including *BOC, CDON, BTRC, CSNK1E, PTCH1, PTCH2, SMO, PRKACA, LATS1, MAPK1*, *NF2*, *MTSS1, WNT10A, WNT3, WNT9a, VEGFA* and *BCL2* as described during *E. chaffeensis* infection. These data demonstrate that the defined TRP120 Hh SLiM activates the Hh signaling pathway and regulates Hh pathway target genes. During *E. chaffeensis* infection, we identified similar Hh activity *in vitro* using the THP-1 cell line as well as *ex vivo* with PHMs. Establishing that the responses observed in the THP-1 cells are similarly observed in PHMs cultured *ex vivo*, which is important because of the limited lifespan of primary cells and the advantages of using THP-1 cell line for functional laboratory studies that may serve as a foundation for understanding mechanisms and potential therapeutics that could be used for treatment in patients.

A TRP120 Hh SLiM targeted antibody blocks Hedgehog signaling.

To elucidate the role of the TRP120 Hh SLiM during *E. chaffeensis* infection, we investigated whether blocking *E. chaffeensis* infection or the TRP120 Hh SLiM with a TRP120 Hh SLiM targeted antibody would inhibit Hh signaling. We used a neutralization assay to determine antibody effects on Hh signaling during *E. chaffeensis* infection or TRP120-Hh-SLiM treatment. *E. chaffeensis* or TRP120-Hh-SLiM were incubated with

306 1.5 µg/mL of either α-TRP120-I1 antibody (targets TRP120 sequence
307 SKVEQEETNPEVLIKDLQDVAS) or α-TRP32 antibody (control) for 1 h and then THP-1
308 cells were subsequently treated with each mixture for 10 h. *E. chaffeensis* infected and
309 TRP120-Hh-SLiM treated cells in the presence of α-TRP120-I1 demonstrated significant
310 reduction in GLI-1 activation relative to *E. chaffeensis*-infected and TRP120-Hh-SLiM
311 treated cells in the presence of α-TRP32 antibody **(Fig. 9A-B)**. These data confirm that
312 the TRP120 Hh SLiM activates GLI-1 and the interaction can be blocked by antibody.

313

314 ***E. chaffeensis* TRP120 Hh SLiM upregulates BCL-2 expression.**
315 During gene expression analysis of the Hh signaling pathway, we observed a significant
316 increase in *BCL2* gene transcription. *BCL2* is one of the major transcriptional targets of
317 the Hh signaling pathway (24). BCL-2 is involved in maintaining mitochondrial
318 membrane integrity and preventing activation of caspases by inhibiting cytochrome-c
319 release from mitochondria, thus inhibiting intrinsic apoptotic pathway (45). Hence, we
320 hypothesized that *E. chaffeensis* activates Hh to upregulate BCL2 to engage an anti-
321 apoptotic cellular program. *E. chaffeensis*-infected **(Fig. 10A),** TRP120-Hh-SLiM- or
322 TRP120-Hh-SLiM-mut-treated **(Fig. 10B)** THP-1 cells were collected for immunoblot to
323 determine BCL-2 levels. Significant upregulation of BCL-2 was detected in *E.*
324 *chaffeensis*-infected and TRP120-Hh-SLiM-treated cells compared to negative controls.
325 Further, we examined the effect of BCL-2 inhibition on *E. chaffeensis* infection using
326 siRNA to individually target and silence *BCL-2* in THP-1 cells. At 24 hpi of *BCL-2*
327 siRNA-transfected cells, *E. chaffeensis* infection (depicted by *dsb* levels) was
328 significantly reduced **(Fig. 10C)**. Collectively, these data suggest that *E. chaffeensis*

329 utilizes its TRP120 Hh SLiM to activate the Hh signaling pathway and upregulate BCL-2
330 for intracellular survival.
331
332 ***E. chaffeensis* mediated activation of Hh signaling inhibits host cell apoptosis.**
333 It is well documented that Hedgehog signaling promotes cell proliferation and prevents
334 cell apoptosis through BCL-2 activation (23, 24, 43). BCL-2 is involved in the inhibition
335 of mitochondria-mediated pro-death pathway (46). Based on our results demonstrating
336 the importance of BCL-2 in *E. chaffeensis* infection, we hypothesized that *E. chaffeensis*
337 activates Hh signaling to inhibit mitochondria-mediated host cell apoptosis via activation
338 of Hh signaling. To examine this hypothesis, infected and uninfected THP-1 cells were
339 treated with Etoposide, an inhibitor of topoisomerase II and inducer of cellular
340 apoptosis, and stained with the JC-1 dye (**Fig. 11A**). *E. ch.*-infected Etoposide-treated
341 THP-1 cells exhibited a significant increase in cells with JC-1 aggregates, suggesting
342 active inhibition of host cell apoptosis during *E. chaffeensis* infection compared to
343 uninfected Etoposide-treated cells. Additionally, there were significantly fewer apoptotic
344 cells in DMSO and Etoposide + *E. chaffeensis* groups, but significantly more apoptotic
345 cells in Etoposide groups, suggesting that *E. chaffeensis* inhibits apoptosis in the
346 presence of Etoposide **(Fig. 11B)**. We further confirmed the loss of mitochondrial
347 membrane potential in the presence of SMO-specific inhibitor Vismodegib in *E.*
348 *chaffeensis*-infected cells using JC-1 dye. The micrograph shows the presence of
349 mitochondria with positive membrane potential in DMSO-treated cells infected with *E.*
350 *chaffeensis* compared to Vismodegib-treated cells infected with *E. chaffeensis* **(Fig.**
351 **11C)**. Additionally, we treated cells with Vismodegib or DMSO and examined cellular

apoptotic state using the Nucview488 and the Mitoview 633 apoptosis assay. During *E. chaffeensis* infection and in the presence of Vismodegib, the Nucview488 dye (a substrate of active caspase 3) translocated to the nucleus, producing green fluorescence in infected cells compared to uninfected cells in the presence of Vismodegib. We did not observe any measurable difference in DMSO-treated uninfected and infected cells **(Fig. 11D)**. These results demonstrate that Hh signaling plays a crucial role during *E. chaffeensis* infection in monocytes by inhibiting an intrinsic death signal.

***E. chaffeensis* induces an apoptotic profile in the presence of Hh inhibitor.**

Our results demonstrate the importance of anti-apoptotic protein BCL-2 during *E. chaffeensis* infection. Additionally, we reveal the vital role that Hh signaling plays during *E. chaffeensis* infection to inhibit apoptosis. Based on our data demonstrating increased Nucview 488 dye in the nucleus of *E. chaffeensis* infected cells in the presence of Vismodegib, we hypothesized that *E. chaffeensis* activates Hedgehog signaling, thus activating BCL-2 to inhibit caspases 9 and 3. To confirm our hypothesis, *E. chaffeensis*-infected and uninfected THP-1 cells were treated with Vismodegib or DMSO (**Fig. 12A**). *E. chaffeensis*-infected Vismodegib-treated THP1 cells demonstrated a significant increase in cytoplasmic condensation (precursor to apoptosis) at 24 hpi compared to uninfected Vismodegib-treated cells and *E. chaffeensis*-infected and uninfected DMSO-treated cells, supporting the conclusion that *E. chaffeensis* activates Hh signaling to prevent apoptosis. Additionally, ehrlichial survival was significantly reduced in the presence of Vismodegib compared to DMSO **(Fig. 12B)**. Further, cell viability

significantly decreased in *E. chaffeensis*-infected cells treated with Vismodegib **(Fig. 11B)**. To define a direct mechanism by which *E. chaffeensis* activates Hedgehog signaling to prevent apoptosis, we evaluated levels of BCL-2, caspase 9 and caspase 3 **(Fig. 12D-F)**. *E. chaffeensis*-infected Vismodegib-treated THP-1 cells showed a significant decrease in BCL-2 at 24 hpi compared to infected DMSO-treated cells **(Fig. 12D)**. In addition, *E. chaffeensis*-infected Vismodegib-treated THP1 cells show a significant decrease in pro-caspases 3 and 9 and a significant increase in cleaved-caspases 3 and 9 at 24 hpi compared to infected DMSO-treated cells **(Fig. 12E-F)**. Collectively, these results define a direct mechanism by which *E. chaffeensis* targets Hh signaling to induce BCL-2 expression, thus preventing intrinsic apoptosis.

Discussion

The Hh pathway was first identified in *Drosophila* in the 1970s and for the last couple of decades, mostly studied in the field of developmental biology (47). More recent investigations have shown Hh role in cell proliferation, differentiation, and inhibition of apoptosis and unregulated activation of Hh signaling results in different hematological malignancies and other cancerous conditions (21, 23, 48, 49). The Hh pathway is targeted by multiple pathogens (18, 19); however, the specific mechanism by which pathogens target Hh signaling through SLiMs has not been reported. In this study, we identified a Hh SLiM within the *E. chaffeensis* TRP120 effector that activates the Hh signaling pathway and inhibits intrinsic host-cell apoptosis to enable infection of the monocyte. This is the first report of a eukaryotic Hh SLiM mimetic in bacterial proteomes, which represents a novel virulence strategy by obligate intracellular bacteria

and extends knowledge regarding eukaryotic cellular signaling motifs that are relevant in pathogen-host interplay. This investigation and other recent reports from our laboratory have provided compelling detail of the molecular mechanisms that *E. chaffeesis* uses to reprogram the host cell using SLiM mimicry. We have identified an array of eukaryotic ligand SLiMs positioned in a single surface expressed effector protein that interface with the host cell and activate Notch, Wnt and now Hh signaling to counter innate defense mechanism and promote infection (7, 9). Collectively, these studies provide the molecular basis of eukaryotic pathway activation by an intracellular pathogen and provides a model that is valuable for understanding how pathogens interface with eukaryotic cells and rewire host cell pathways for infection.

The Hh pathway has been implicated in various human diseases including several types of cancers (21, 23, 40). Notably, several recent studies have reported increased levels of Hh signaling in response to various pathogens (19, 50-52). An elevated level of Hh signaling was reported in cells infected with Hepatitis B and C virus (HBV and HCV, respectively), and hepatocytes from patients with chronic HBV and HCV infection displayed an increased production of Hh ligands and an accumulation of Hh-responsive cells with higher levels of pathway activity (50). Additionally, studies demonstrate that the *in vitro* treatment of hepatocytes with whole HBV replicon increases expression of Hh target genes in a GLI-dependent manner and viral protein HBV X stabilizes GLI-1 and promotes its nuclear accumulation (52). Although a precise mechanism by which Hh signaling promotes HBV and HCV infections remains unclear, Hh activation in hepatocytes appears to promote HCV infection, indicating the presence of a positive

421 feedback loop between pathway activation and virus production (53). In addition,
422 *Mycobacterium* species appear to mediate Hh signaling. *M. bovis* upregulates Shh-
423 PI3K-mTOR-NF-κB signaling in human dendritic cells to activate BCG-induced Treg
424 expansion. Interestingly, *M. bovis* relies heavily on Hh signaling, while Notch signaling
425 hindered the ability of the infected dendritic cells to expand Tregs and Wnt signaling
426 demonstrated no affect (51).
427
428 *Ehrlichia chaffeensis* TRP120 is a moonlighting protein involved in modulating various
429 cellular processes (54) and has evolved Wnt and Notch SLiMs to activate the conserved
430 cellular signaling pathways (7, 9). In a recent report demonstrating Notch activation
431 during *E. chaffeensis* infection, we determined *GLI-1* gene expression was activated by
432 a Notch ligand SLiM in the TRP120 TR (4). The intricate crosstalk between Wnt, Notch,
433 and Hh signaling is well defined; thus, we investigated the possibility of additional ligand
434 SliMs and Hh pathway activation during *E. chaffeensis* infection (35). Utilizing similar *in*
435 *silico* analysis, a potential TRP120 Hh SLiM was predicted within the TRP120 TRD with
436 significant homology to a region of Hh ligands at the Hh ligand-PTCH receptor binding
437 site (37). Using iRNA, we demonstrated that *E. chaffeensis* relies on PTCH2, but not
438 PTCH1 for survival. Although PTCH1 and PTCH2 share overlapping functions (55),
439 PTCH1 contains an ubiquitin ligase binding site within its C-terminal tail, making it less
440 stable than PTCH2, which may make PTCH1 less favorable to TRP120 (56). We
441 determined that TRP120 TRD interacts directly and has strong binding affinity (nM
442 range) with PTCH2. Moreover, multiple studies have investigated the affinity of Hh
443 ligands to PTCH receptors and reported ligand affinity for PTCH1 (Shh, 1.0 nM; Dhh,

2.6 nM; Ihh, 1.0 nM) and PTCH2 (Shh, 1.8 nM; Dhh, 0.6 nM; Ihh, 0.4 nM) (57). Interestingly, Shh binds PTCH2 with stronger affinity, while Dhh and Ihh bind PTCH1 with stronger affinity. TRP120 may bind PTCH2 similarly to Shh in our model, since Shh is highly expressed in THP-1 cells compared to Dhh and Ihh and has a greater affinity to PTCH2. Further, the affinity of endogenous Hh ligands for PTCH2 is strong, but surprisingly weaker than what was exhibited by TRP120 (4.40 ± 1.5 nM). A recent study demonstrates that ligands with higher binding affinity disable lower affinity ligands from binding their receptor (58). Thus, TRP120 may have a higher binding affinity to PTCH2 to provide a competitive advantage over endogenous Hh ligands.

We investigated whether TRP120 is directly responsible for activating Hh signaling during infection. Indeed, we confirmed that TRP120 induces nuclear translocation of GLI-1 and transcriptional induction of Hh pathway genes including crucial components of the Hh-signaling pathway such as PTCH2, SMO, and GLI-1. Although there was differential expression of Hh pathway genes in TRP120 treated and Shh ligand treated THP-1 cells, we discovered that more than 50% of genes were common during TRP120 and Shh treatment, which supports TRP120 as a Hh ligand mimic. Differences between TRP120 and Shh are expected, since there are differing biological functions between Shh, Dhh and Ihh ligands despite a highly similar amino acid sequence (59). Additionally, TRP120 also contains Wnt and Notch SLiMs which may influence gene expression due to the intricate crosstalk between the pathways. For example, Notch signaling directly regulates effector and target molecules of the Hedgehog signaling pathway (60). Additionally, Wnt signaling increases GLI-1 transcriptional activity (61),

467 which suggests that TRP120 can regulate Hh signaling in various ways. In addition, we
468 concluded that the predicted TRP120 Hh SLiM peptide is sufficient in activating Hh
469 signaling. Here, we established a model of eukaryotic protein mimicry where the
470 TRP120 Hh SLiM is functional and activates the Hh signaling pathway and Hh gene
471 targets in a concentration dependent manner. In our experiments, the TRP120 Hh SLiM
472 demonstrated stronger upregulation of Hh gene targets than full length TRP120. This is
473 likely related to the molar concentration of SLiM sequences present in each treatment.
474 The actual amount of SLiM added using rTRP120 is substantially less than the
475 concentration of peptide SLiM used. Nevertheless, there were similar and consistent Hh
476 gene activation profiles observed with *E. chaffeensis,* TRP120 and TRP120 Hh SLiM.
477 The TRP120 Hh SLiM has sequence homology with the N-terminal region of Shh, which
478 is responsible for binding PTCH receptors (62). However, the amino acid residues
479 important for Shh-PTCH2 interactions have not been well defined. Our findings
480 demonstrate that mutations in the homology sequence between TRP120 and Hh
481 ligands results in deactivation of Hh signaling, which indicates that these amino acid
482 residues may be critical in Hh ligand-PTCH2 binding and subsequent GLI-1 activation.
483 To further support our results, we used an antibody that would recognize and block the
484 TRP120 Hh SLiM. Indeed, we determined that antibody binding and blocking of the Hh
485 SLiM inhibits both *E. chaffeensis* and TRP120 Hh SLiM activation of Hh signaling.
486 These experiments also demonstrate that the TRP120 Hh SLiM is the only Hh mimietic
487 utilized by *E. chaffeensis,* since the antibody blocked GLI-1 activation in SLiM treated
488 and *E. chaffeensis* infected groups.
489

In the past year, our laboratory has demonstrated that TRP120 contains multiple SLiMs that activate Hh, Notch and Wnt signaling, which likely work together to promote infection due to the well-known but complex crosstalk between Hh, Notch and Wnt pathways (60). Each TRP120 SLiM is found within the intrinsically disordered TRD within close proximity, suggesting that the TRD has a primary and potentially unique role in SLiM mimicry (7, 9). TRDs are often identified in bacterial proteins with critical functions for pathogenicity (63). For example, *Xanthomonas* secreted TAL effectors contain repeats, which facilitate DNA binding and gene regulation (64, 65). Similarly, we have identified DNA binding capability in the TR domain of TRP120 (11). SLiMs drive evolution and rapidly evolve *ex nihilo* to add new functionality to proteins. Pathogens are known to convergently evolve SLiMs within disordered regions due to the limited number of mutations necessary for the generation of a new SLiM (66). SLiMs contain high evolutionary plasticity due to their disordered nature, short length and limited number of specificity-determining residues (67). Thus, it appears that *E. chaffeensis* has evolved TRP120 SLiMs through convergent evolution to increase complexity necessary for engaging multiple cellular signaling pathways. All presently defined SLiMs acquired by TRP120 activate conserved signaling pathways known to prevent apoptosis, which may be a strategy utilized by *E. chaffeensis* to assure host-cell survival for the *Ehrlichia* life cycle.

During microbial infection, cellular apoptosis plays an important role as a host defense mechanism, as it minimizes infection and contributes to protective immunity through processing apoptotic bodies containing infected microbes to facilitate antigen

presentation (29). Intracellular bacteria usually require several days of replication in a host cell before being released to infect neighboring cells. Thus, pathogens like *Mycobacterium, Chlamydia, Rickettsia, Anaplasma,* and others have evolved multiple mechanisms to inhibit host cell apoptosis (68-72). Intracellular pathogens regulate host cell apoptosis to modulate the host immune defenses in a variety of ways, including regulation of the mitochondria-mediated intrinsic apoptosis pathway (28, 29, 73). For instance, *E. chaffeensis* utilizes the Type IV secretion system (T4SS) effector Etf-1 to enter the mitochondria and inhibit mitochondria-mediated intrinsic apoptosis in host cells (74). T4SS effectors are well known for their virulence role in preventing apoptosis during infection (75). However, there are many mechanisms pathogens exploit to inhibit apoptosis. Notably, in this study we demonstrate a novel mechanism associated with a T1SS effector capable of inhibiting apoptosis. We reveal that TRP120 significantly increases BCL2 expression via its Hh SLiM, thus preventing host intrinsic apoptosis signaling which promotes ehrlichial infection. Additionally, siRNAs against *BCL-2* significantly reduced ehrlichial load, suggesting that Hh regulated BCL-2 anti-apoptotic mechanisms are an important component of an anti-apoptotic strategy by *Ehrlichia.* Notably, *in vitro* studies demonstrate the upregulation of BCL-2 and in host macrophages during *Mycobacterium tuberculosis* infection to prevent apoptosis for intracellular survival (76). Additionally, *Mycobacterium tuberculosis* secretes PtpA to dephosphorylate host protein GSK3 and suppresses caspase 3 during early infection to prevent host-cell apoptosis (77). Interestingly, GSK3 is well known for its role during Hh signaling by regulating GLI (78).

Hh signaling plays a critical role in promoting differentiation, proliferation and maturation, and preventing apoptosis of different immune cells, including monocytes and macrophages (79, 80). A small molecule Hh inhibitor of the cell surface receptor SMO (Vismodegib) confirmed that the Hh pathway inhibits apoptosis and is required for ehrlichial survival. We confirmed that loss of Hh signaling during ehrlichial infection induces the intrinsic apoptotic pathway. Specifically, we conclude that *E. chaffeensis* activates BCL-2 to prevent intrinsic apoptosis by maintaining the integrity of the mitochondrial membrane, preventing the release of cytochrome c, and activation of caspase 9 and caspase 3. These results reveal a novel mechanism by which *E. chaffeensis* modulates the Hh pathway for infection by extending the host cell lifespan, which is consistent with the role of this pathway in cell biology.

Diving deeper into understanding the molecular mechanisms of *E. chaffeensis* pathogenesis in modulating complex cellular processes will help in developing next-generation therapeutics, specifically aimed at mechanistically defined host targets. The current study reveals a novel mechanism where *E. chaffeensis* utilizes SLiM ligand mimicry to activate Hh signaling in the host, thus modulating the intrinsic apoptotic signal as depicted in **Fig. 13**. Hence, this study reveals the importance of the Hh signaling pathway in ehrlichial intracellular growth and developmental cycle and provides a new target for the development of a novel therapeutic approach against ehrlichial infection that may be applicable to other intracellular pathogens, in which exploitation of such conserved cellular pathways is necessary for infection.

559 **Materials and Methods**

560

561 **Cell culture and *E. chaffeensis* cultivation.**

562 Human monocytic leukemia cells (THP-1; ATCC TIB-202) or primary human monocytes
563 (PHMs) were propagated in RPMI 1640 with L-glutamine and 25 mM HEPES buffer
564 (Invitrogen, Carlsbad, CA), supplemented with 1 mM sodium pyruvate (Sigma-Aldrich,
565 St. Louis, MO), 2.5 g/liter D-(+)-glucose (Sigma-Aldrich), and 10% fetal bovine serum at
566 37°C in a 5% CO_2 atmosphere. Human primary monocytes were isolated using MACS
567 negative selection (Miltenyi Biotec, Cambridge, MA) from peripheral blood mononuclear
568 cells obtained from healthy human donors (de-identified) (Gulf Coast Regional Blood
569 Center, Houston, TX). *Ehrlichia chaffeensis* (Arkansas strain) was cultivated in THP-1
570 cells as previously described (81). Cells were harvested with 30% confluency for
571 confocal microscopy and 100% confluency for all other experiments.

572

573 **Protein sequence analysis.**

574 The TRP120 protein sequence (NCBI gene accession number AAO12927.1) and
575 Dhh/Ihh/Shh *Homo sapiens* protein sequences (NCBI gene accession numbers
576 NP_066382/ NP_002172/ NP_000184.1) were analyzed by the NCBI Protein Basic
577 Local Alignment Search Tool (Protein BLAST) for sequence alignment.

578 **Informational spectrum method analysis.**

579 Informational spectrum method (ISM) *in-silico* analysis was performed by the Biomed
580 Protection (biomedprotection.com) using a wEB platform and described in detail
581 previously (7).

582

583 **Recombinant proteins and peptides.**

584 *E. chaffeensis* recombinant full length TRP120 (rTRP120-FL), TRP120 TRD (rTRP120-
585 TR) or thioredoxin (rTrx; ctrl) were expressed in *E. coli* and purified as described
586 previously (4). rTRP120 is a Trx-fusion protein; therefore, rTrx was used as a negative
587 control. rShh (R&D Systems, Minneapolis, MN) and rPTCH2 (MyBioSource, San Diego,
588 CA) were obtained from a commercial source. Shh was selected as a positive control
589 since it is normally expressed in THP-1 cells, while Dhh and Ihh are not (The Human
590 Protein Atlas; www.proteinatlas.org). Peptides were commercially synthesized
591 (GenScript, Piscataway, NJ) for TRP120-TR-Hh (VSKVEQEKTNPEVLIKDLQD;
592 contains the homologous Hh sequence), TRP120-TR (-)
593 (SHQGETEKESGITESHQKEDEI; neg ctrl) , TRP120-Hh-SLiM (NPEVLIKD), and
594 TRP120-Hh-SLiM-mut (SKVEQEKTGAGAGAGALQ; Gln/Ala substitutions in the Hh
595 SLiM motif).

596

597 **Antibodies and inhibitors.**

598 Antibodies used in this study include α-DSB (82), α-TRP120-I1 (targets TRP120
599 sequence SKVEQEETNPEVLIKDLQDVAS) (83), α-TRP32 (84), α -GLI-1/2/3 (Santa
600 Cruz Biotechnology, Dallas, TX), α-SHH (Cell Signaling, Danvers, MA), α-SUFU (Cell

Signaling), α-PTCH1/2 (Cell Signaling), α-SMO (Sigma-Aldrich), α-BCL-2 (Cell Signaling), α-Caspase 3 (Cell Signaling), α-Caspase 9 (Sell Signaling), α-GAPDH (MilliporeSigma, Burlington, MA) and α-PCNA (Cell Signaling). Inhibition of the Hh-signaling pathway was performed using Vismodegib/GDC0499 (Selleckchem, Houston, TX).

RNA interference.

THP-1 cells (1.0×10^6) were transfected with human siRNA (10 nM) using Lipofectamine 3000 (Invitrogen, Waltham, MA). All siRNAs were ON-TARGETplus SMARTpool (Dharmacon, Lafayette, Co). Briefly, specific siRNA (3 µl) and Lipofectamine 3000 reagent (7.5 µl) were added to the Opti-MEM medium (250 µl) (Invitrogen), incubated for 5 min at room temperature, and then added to the cell suspension in a 6-well plate. Scrambled iRNA was used as a control in uninfected and infected samples. Post-transfection (24 h), cells were infected with cell-free *E. chaffeensis* (MOI 100). Cells were harvested at 24 hpi to and ehrlichial load determined using qPCR as described previously (85). All knockdowns were performed with three biological and technical replicates and significance determined using a *t*-test analysis.

Transfection and immunofluorescent microscopy.

HeLa cells were transfected with plasmid using Lipofectamine 2000 (Invitrogen) according to the manufacturer's protocol. Cells ectopically expressing TRP120 were imaged by immunofluorescent microscopy as described previously (86). Intensity

623 correlation analysis (ICA) and corrected total cell florescence (CTCF) were measured
624 using ImageJ (87, 88).
625
626 **Co-Immunoprecipitation (Co-IP).**
627 Interactions between TRP120 and PTCH2 were determined by Co-IP using the Thermo
628 Scientific Pierce Crosslink IP Kit (#26147). THP-1 cells (100% confluent) were infected
629 with *E. chaffeensis* at an MOI of 100 for 24 h. The cells were harvested, and Co-IPs
630 were performed with TRP120-I1 and PTCH2 antibodies according to the manufacturer's
631 protocol. Immunoprecipitated eluates and starting input lysates were processed for
632 Western blotting and probed for TRP120 or PTCH2. IP control antibody included IgG
633 purified from normal rabbit serum with Melon Gel IgG Spin Purification Kit (Thermo
634 Scientific, Rockford, IL). The Co-IPs performed in triplicate.
635
636 **Surface plasmon resonance (SPR).**
637 SPR was used to investigate binding kinetics of rTRP120 tandem repeat domain
638 (TRP120-TR) and rPTCH2 and performed as described previously (7). Briefly, SMFS-
639 AFM was used to directly extract energetic, thermodynamic and kinetic parameters from
640 force curves describing the TRP120-PTCH2 receptor binding free-energy landscape.
641 rPTCH2 was immobilized on a nickel chip followed by the injection of an analyte
642 solution containing solubilized rTRP120-TR or rTrx (-) to determine the binding affinity
643 on a Biacore T100. Constant injection of rTRP120-TR provided a quantified
644 readout derived from the change in mass on the surface of the chip as rTRP120-TR
645 binds rPTCH2 at a constant rate until reaching equilibrium. The unbinding forces were

plotted as a function of the loading rate; from this plot we extracted the dissociation rate (koff) and the energy barrier width xu (nm). The kinetic on-rate, kon, was obtained by varying the dwell time of the TRP120-functionalized tip on cell surfaces, thereby determining binding probability. Using these parameters, we quantified the ΔG of interaction. The results were expressed as the means ± standard deviation (SD) of data obtained from three independent experiments. rTrx fusion protein was used as the negative control since it has no effect on Hh signaling. The binding affinity (K_D) was determined for TRP120-PTCH2 interaction by extracting the association rate constant and dissociation rate constant from the sensorgram curve (K_D = Kd/Ka).

Confocal microscopy.

Ehrlichia chaffeensis-infected and uninfected THP-1 cells were seeded in T-75 flasks (Corning, Lowell, MA) and collected at 0, 2, 4, 10, 24 and 48 hpi. rTRP120-FL, rTrx, rShh, TRP120-TR-Hh, TRP120-TR (-), TRP120-Hh-SLiM and TRP120-Hh-SLiM-mut peptide-stimulated THP-1 cells were collected at 6 hpt. Experiments performed with at least three biological and technical replicates. THP-1 samples (non-adherent) were washed twice and adhered to glass slides by cytocentrifugation (1000 RPM for 5 min). Uninfected, *E. chaffeensis*-infected, rTRP120-FL-, rTrx-, rShh-, and TRP120-Hh-SLiM and TRP120-Hh-SLiM-mut peptide-treated PHMs were seeded in 12-well plates (Corning, Lowell, MA) containing a coverslip and incubated for 10 h. After incubation, PHMs were washed twice with phosphate buffered saline (PBS). THP-1 cells and PHMs were fixed with 4% paraformaldehyde (PFA) for 20 min at room temperature followed by three subsequent washes in PBS. Fixed cells were blocked and permeabilized with

669 0.3% Triton X-100 in 2% BSA for 30 min and washed. The cells were then incubated
670 subsequently with a mouse monoclonal GLI-1 primary antibody (1:200) and in-house
671 rabbit DSB serum in blocking buffer (PBS with 2% BSA) for 1 h, with PBS washes (3X)
672 after each treatment. Cells were incubated with Alexa Fluor-conjugated secondary
673 antibodies goat α-mouse and goat α-rabbit (Thermo Fisher) diluted 1:200 in blocking
674 buffer for 30 min and mounted with ProLong Gold Antifade with DAPI (4′,6-diamidino-2-
675 phenylindole; Thermo Fisher). Confocal laser micrographs were obtained with Zeiss
676 LSM 880 laser microscope and analyzed with Zen black and Fiji software. For confocal
677 analysis, randomized areas/slide (n=10) were used to detect GLI-1 nuclear
678 translocation.
679
680 **RNA isolation and cDNA synthesis.**
681 Uninfected, *E. chaffeensis*-infected, rTRP120-FL, rShh, TRP120-Hh-SLiM peptide and
682 TRP120-Hh-SLiM-mut peptide-stimulated THP-1 cells were harvested at different time
683 points and data was generated from three biological and technical replicates. *E.*
684 *chaffeensis* infection was collected at 4, 8, 24 and 48 hpi at MOI 100. THP-1 cells were
685 incubated with 50, 500 ng/mL or 1 µg/mL of peptide or recombinant protein and
686 harvested at 24 hpt. rTrx (-) or uninfected/untreated cells were used as controls for
687 infection, and protein and peptide treatments to determine fold-change. Total RNA was
688 isolated from each sample (10^6 cells/sample) using RNeasy Mini kit (Qiagen, Hilden,
689 Germany). On column DNA digestion was performed using the RNase-free DNase kit
690 (Qiagen). The concentration and the purity of RNA were determined using a Nanodrop
691 100 spectrophotometer (Thermo Fisher Scientific). cDNA was synthesized from total

692 RNA (1.0 µg) using iScript cDNA Synthesis Kit (BioRad, Hercules, CA) according to the
693 manufacturer's protocol.
694
695 **Human Hh signaling pathway PCR array.**
696 The human Hh signaling target PCR array (Qiagen) profiled the expression of 84 key
697 genes responsive to Hh signal transduction, that includes receptors, ligands, and
698 transcription factor/co-factors, and known target genes. PCR arrays were performed
699 according to the PCR array handbook from the manufacturer (Qiagen). Real-time PCR
700 was performed using RT^2 Profiler PCR array in combination with RT^2 SYBR green
701 master mix (Qiagen) using a QuantStudio 6 Flex real-time PCR system. PCR conditions
702 and analysis were conducted as previously described (7). The red, black and green dots
703 in the volcano plot represent upregulation (≥ 2), no change or down-regulation (≤ -2),
704 respectively for a given gene on the array. The horizontal blue lines on the volcano plots
705 determine the level of significance ($p \leq 0.05$).
706
707 **Western immunoblot analysis.**
708 For Western blots, THP-1 cells were harvested and washed twice with PBS and lysates
709 were prepared using CytoBuster protein extraction reagent (Novagen/EMD, Gibbstown,
710 NJ) supplemented with complete mini EDTA-free protease inhibitor (Roche, Basel,
711 Switzerland), phenylmethene-sulfonylfluoride PMSF (10 mM) (Sigma-Aldrich). The cell
712 lysates were centrifuged at 15,000*g* for 10 min at 4°C. The supernatants were collected,
713 and protein concentration was then measured using Pierce BCA Protein Assay Kit
714 (Thermo Fisher Scientific, Waltham, MA). Equal amounts of protein (15-30 µg/well)

were separated by sodium dodecyl sulfate-polyacrylamide gel electrophoresis (SDS-PAGE), transferred to nitrocellulose membrane and immunoblotted with primary antibodies. Horseradish peroxidase-conjugated goat anti-rabbit or goat anti-mouse IgG (H+L) secondary antibodies (Kirkegaard & Perry Laboratories, Gaithersburg, MD) were used and visualized by SuperSignal West Dura chemiluminescent substrate or ECL (Thermo Fisher Scientific). All Western blots were performed with at least three biological and technical replicates and significance determined by *t*-test analysis.

Mitochondrial membrane potential assay.

To confirm *E. chaffeensis*-mediated inhibition of host cell apoptosis, infected and uninfected THP-1 cells were treated with DMSO (- control) or Etoposide (100 µm) (Selleckchem), an inhibitor of topoisomerase II and inducer of cellular apoptosis, for 24 h and stained with a JC-1 Mitochondrial Membrane Potential Detection Kit using the manufacturers protocol (Biotium, Fremont, CA). The dye forms JC aggregates (orange; 590±17.5nm) in mitochondria with positive membrane potential in normal cells. Inversely, due to depolarization of the mitochondrial membrane in apoptotic cells, JC-1 remains as a monomer and yields green fluorescence (emission of 530±15nm). To inhibit Hh signaling, THP-1 cells were treated with a SMO-specific inhibitor Vismodegib (200 nM) for 24 h. NucView® 488 & MitoView™ 633 Apoptosis Assay Kit was utilized to examine cellular apoptotic state using the manufacturers protocol (Biotium). A micrograph was used to demonstrate that the Nucview488 dye (a substrate of active caspase 3) is cleaved by caspase 3/7 and produces green fluorescence due to the

737 activation of the cellular apoptotic pathway. Experiments were performed with at least
738 three biological and technical replicates.
739
740 **Hh inhibitor infection analysis.**
741 THP-1 cells were treated with Vismodegib or DMSO (200 nM) and infected with *E.*
742 *chaffeensis* (MOI 50) for 24 h. THP-1 cells were harvested for Western blot (as
743 described) and Diff-Quik staining (Fisher Scientific). Ehrlichial load was determined
744 using qPCR as described previously (85). Cell viability and count were measured with
745 the Cellometer mini (Nexcelom) with preinstalled normal and *E. chaffeensis*-infected
746 THP-1 cell profiles. Cellometer Mini uses bright field imaging and pattern-recognition
747 software to count and define individual live cells and dead cells stained with Trypan
748 Blue. An analysis summary is produced, including a Trypan blue cell count,
749 concentration, diameter, and % viability. At least three biological and technical
750 replicates were performed.

Acknowledgments

We thank the UTMB Solution Biophysics Laboratory and the Optical Microscopy Core for assistance with confocal microscopy. This work was supported by the National Institute of Allergy and Infectious Disease grants AI137779 and AI149136 to J.W.M., McLaughlin Endowment and T32AI007526-20 Biodefense Training Program predoctoral fellowships to C.D.B., NIH 1F31AI152424 predoctoral fellowship to L.L.P, and Sealy Center for Vector Borne and Zoonotic Diseases predoctoral fellowship to N.A.P.

References

1. Zhang JZ, Popov VL, Gao S, Walker DH, Yu XJ. The developmental cycle of *Ehrlichia chaffeensis* in vertebrate cells. Cell Microbiol. 2007;9(3):610-8.
2. Lina TT, Farris T, Luo T, Mitra S, Zhu B, McBride JW. Hacker within! *Ehrlichia chaffeensis* Effector Driven Phagocyte Reprogramming Strategy. Frontiers in cellular and infection microbiology. 2016;6.
3. Luo T, Kuriakose JA, Zhu B, Wakeel A, McBride JW. *Ehrlichia chaffeensis* TRP120 interacts with a diverse array of eukaryotic proteins involved in transcription, signaling, and cytoskeleton organization. Infect Immun. 2011;79(11):4382-91.
4. Lina TT, Dunphy PS, Luo T, McBride JW. Ehrlichia chaffeensis TRP120 Activates Canonical Notch Signaling To Downregulate TLR2/4 Expression and Promote Intracellular Survival. mBio. 2016;7(4).
5. Dunphy PS, Luo T, McBride JW. *Ehrlichia chaffeensis* Exploits Host SUMOylation Pathways to Mediate Effector-Host Interactions and Promote Intracellular Survival. Infect Immun. 2014.
6. Zhu B, Das S, Mitra S, Farris TR, McBride JW. *Ehrlichia chaffeensis* TRP120 moonlights as a HECT E3 ligase involved in self and host ubiquitination to influence protein interactions and stability for intracellular survival. Infect Immun. 2017.
7. Rogan MR, Patterson LL, Byerly CD, Luo T, Paessler S, Veljkovic V, et al. Ehrlichia chaffeensis TRP120 Is a Wnt Ligand Mimetic That Interacts with Wnt Receptors and Contains a Novel Repetitive Short Linear Motif That Activates Wnt Signaling. mSphere. 2021;6(2).
8. Wang JY, Zhu B, Patterson LL, Rogan MR, Kibler CE, McBride JW. Ehrlichia chaffeensis TRP120-mediated ubiquitination and proteasomal degradation of tumor suppressor FBW7 increases oncoprotein stability and promotes infection. PLoS Pathog. 2020;16(4):e1008541.
9. LaNisha L. Patterson TSV, Caitlan D. Byerly, Duc Cuong Bui, Jignesh Patel, Veljko Veljkovic, Slobodan Paessler, Jere W. McBride. Ehrlichia SLiM ligand mimetic activates Notch signaling in human monocytes. bioRxiv. 2022;01.13.476283.
10. Luo T, Dunphy PS, Lina TT, McBride JW. *Ehrlichia chaffeensis* Exploits Canonical and Noncanonical Host Wnt Signaling Pathways to Stimulate Phagocytosis and Promote Intracellular Survival. Infect Immun. 2015.
11. Zhu B, Kuriakose JA, Luo T, Ballesteros E, Gupta S, Fofanov Y, et al. Ehrlichia chaffeensis TRP120 binds a G+C-rich motif in host cell DNA and exhibits eukaryotic transcriptional activator function. Infect Immun. 2011;79(11):4370-81.
12. Zhu B, Das S, Mitra S, Farris TR, McBride JW. Ehrlichia chaffeensis TRP120 Moonlights as a HECT E3 Ligase Involved in Self- and Host Ubiquitination To Influence Protein Interactions and Stability for Intracellular Survival. Infect Immun. 2017;85(9).
13. Davey NE, Trave G, Gibson TJ. How viruses hijack cell regulation. Trends Biochem Sci. 2011;36(3):159-69.
14. Samano-Sanchez H, Gibson TJ. Mimicry of Short Linear Motifs by Bacterial Pathogens: A Drugging Opportunity. Trends Biochem Sci. 2020;45(6):526-44.
15. Armas-Lopez L, Zuniga J, Arrieta O, Avila-Moreno F. The Hedgehog-GLI pathway in embryonic development and cancer: implications for pulmonary oncology therapy. Oncotarget. 2017;8(36):60684-703.

16. Ingham PW, McMahon AP. Hedgehog signaling in animal development: paradigms and principles. Genes & development. 2001;15(23):3059-87.
17. Lee RT, Zhao Z, Ingham PW. Hedgehog signalling. Development. 2016;143(3):367-72.
18. Lan X, Wen H, Cheng K, Plagov A, Marashi Shoshtari SS, Malhotra A, et al. Hedgehog pathway plays a vital role in HIV-induced epithelial-mesenchymal transition of podocyte. Experimental cell research. 2017;352(2):193-201.
19. Smelkinson MG. The Hedgehog Signaling Pathway Emerges as a Pathogenic Target. J Dev Biol. 2017;5(4).
20. Taipale J, Cooper MK, Maiti T, Beachy PA. Patched acts catalytically to suppress the activity of Smoothened. Nature. 2002;418(6900):892-7.
21. Irvine DA, Copland M. Targeting hedgehog in hematologic malignancy. Blood. 2012;119(10):2196-204.
22. Yang L, Xie G, Fan Q, Xie J. Activation of the hedgehog-signaling pathway in human cancer and the clinical implications. Oncogene. 2010;29(4):469-81.
23. Jia Y, Wang Y, Xie J. The Hedgehog pathway: role in cell differentiation, polarity and proliferation. Arch Toxicol. 2015;89(2):179-91.
24. Han ME, Lee YS, Baek SY, Kim BS, Kim JB, Oh SO. Hedgehog signaling regulates the survival of gastric cancer cells by regulating the expression of Bcl-2. Int J Mol Sci. 2009;10(7):3033-43.
25. Behar SM, Briken V. Apoptosis inhibition by intracellular bacteria and its consequence on host immunity. Curr Opin Immunol. 2019;60:103-10.
26. Strasser A, O'Connor L, Dixit VM. Apoptosis signaling. Annu Rev Biochem. 2000;69:217-45.
27. Ashida H, Mimuro H, Ogawa M, Kobayashi T, Sanada T, Kim M, et al. Cell death and infection: a double-edged sword for host and pathogen survival. The Journal of cell biology. 2011;195(6):931-42.
28. Rudel T, Kepp O, Kozjak-Pavlovic V. Interactions between bacterial pathogens and mitochondrial cell death pathways. Nature reviews Microbiology. 2010;8(10):693-705.
29. Lamkanfi M, Dixit VM. Manipulation of host cell death pathways during microbial infections. Cell host & microbe. 2010;8(1):44-54.
30. Bigelow RL, Chari NS, Unden AB, Spurgers KB, Lee S, Roop DR, et al. Transcriptional regulation of bcl-2 mediated by the sonic hedgehog signaling pathway through gli-1. J Biol Chem. 2004;279(2):1197-205.
31. Murphy KM, Ranganathan V, Farnsworth ML, Kavallaris M, Lock RB. Bcl-2 inhibits Bax translocation from cytosol to mitochondria during drug-induced apoptosis of human tumor cells. Cell Death Differ. 2000;7(1):102-11.
32. Williams NM, Timoney PJ. In vitro killing of *Ehrlichia risticii* by activated and immune mouse peritoneal macrophages. Infection & Immunity. 1993;61(3):861-7.
33. Zhang JZ, Sinha M, Luxon BA, Yu XJ. Survival strategy of obligately intracellular *Ehrlichia chaffeensis*: novel modulation of immune response and host cell cycles. InfectImmun. 2004;72(1):498-507.
34. Rikihisa Y. Molecular events involved in cellular invasion by *Ehrlichia chaffeensis* and *Anaplasma phagocytophilum*. VetParasitol. 2010;167(2-4):155-66.

35. Kling JC, Blumenthal A. Roles of WNT, NOTCH, and Hedgehog signaling in the differentiation and function of innate and innate-like lymphocytes. Journal of leukocyte biology. 2016.
36. Degirmenci B, Valenta T, Dimitrieva S, Hausmann G, Basler K. GLI1-expressing mesenchymal cells form the essential Wnt-secreting niche for colon stem cells. Nature. 2018;558(7710):449-53.
37. Gong X, Qian H, Cao P, Zhao X, Zhou Q, Lei J, et al. Structural basis for the recognition of Sonic Hedgehog by human Patched1. Science. 2018;361(6402).
38. Veljkovic V, Glisic S, Muller CP, Scotch M, Branch DR, Perovic VR, et al. In silico analysis suggests interaction between Ebola virus and the extracellular matrix. Front Microbiol. 2015;6:135.
39. Jimenez-Sanchez M, Menzies FM, Chang YY, Simecek N, Neufeld TP, Rubinsztein DC. The Hedgehog signalling pathway regulates autophagy. Nat Commun. 2012;3:1200.
40. Xu XF, Guo CY, Liu J, Yang WJ, Xia YJ, Xu L, et al. Gli1 maintains cell survival by up-regulating IGFBP6 and Bcl-2 through promoter regions in parallel manner in pancreatic cancer cells. J Carcinog. 2009;8:13.
41. Rikihisa Y. Subversion of RAB5-regulated autophagy by the intracellular pathogen *Ehrlichia chaffeensis*. Small GTPases. 2017:1-7.
42. Svard J, Heby-Henricson K, Persson-Lek M, Rozell B, Lauth M, Bergstrom A, et al. Genetic elimination of Suppressor of fused reveals an essential repressor function in the mammalian Hedgehog signaling pathway. Developmental cell. 2006;10(2):187-97.
43. Ruiz i Altaba A, Sanchez P, Dahmane N. Gli and hedgehog in cancer: tumours, embryos and stem cells. Nature reviews Cancer. 2002;2(5):361-72.
44. Humke EW, Dorn KV, Milenkovic L, Scott MP, Rohatgi R. The output of Hedgehog signaling is controlled by the dynamic association between Suppressor of Fused and the Gli proteins. Genes & development. 2010;24(7):670-82.
45. Soriano ME, Scorrano L. The interplay between BCL-2 family proteins and mitochondrial morphology in the regulation of apoptosis. Advances in experimental medicine and biology. 2010;687:97-114.
46. Zhang J-z, Sinha M, Luxon BA, Yu X-j. Survival Strategy of Obligately Intracellular Ehrlichia chaffeensis: Novel Modulation of Immune Response and Host Cell Cycles. Infection and immunity. 2004;72(1):498-507.
47. Nusslein-Volhard C, Wieschaus E. Mutations affecting segment number and polarity in Drosophila. Nature. 1980;287(5785):795-801.
48. Aberger F, Kern D, Greil R, Hartmann TN. Canonical and noncanonical Hedgehog/GLI signaling in hematological malignancies. Vitam Horm. 2012;88:25-54.
49. Campbell V, Copland M. Hedgehog signaling in cancer stem cells: a focus on hematological cancers. Stem Cells Cloning. 2015;8:27-38.
50. Pereira Tde A, Witek RP, Syn WK, Choi SS, Bradrick S, Karaca GF, et al. Viral factors induce Hedgehog pathway activation in humans with viral hepatitis, cirrhosis, and hepatocellular carcinoma. Laboratory investigation; a journal of technical methods and pathology. 2010;90(12):1690-703.
51. Holla S, Stephen-Victor E, Prakhar P, Sharma M, Saha C, Udupa V, et al. Mycobacteria-responsive sonic hedgehog signaling mediates programmed death-ligand 1- and prostaglandin E2-induced regulatory T cell expansion. Sci Rep. 2016;6:24193.

52. Kim HY, Cho HK, Hong SP, Cheong J. Hepatitis B virus X protein stimulates the Hedgehog-Gli activation through protein stabilization and nuclear localization of Gli1 in liver cancer cells. Cancer letters. 2011;309(2):176-84.
53. Choi SS, Bradrick S, Qiang G, Mostafavi A, Chaturvedi G, Weinman SA, et al. Up-regulation of Hedgehog pathway is associated with cellular permissiveness for hepatitis C virus replication. Hepatology. 2011;54(5):1580-90.
54. Byerly CD, Patterson LL, McBride JW. Ehrlichia TRP effectors: moonlighting, mimicry and infection. Pathog Dis. 2021;79(5).
55. Zhulyn O, Nieuwenhuis E, Liu YC, Angers S, Hui CC. Ptch2 shares overlapping functions with Ptch1 in Smo regulation and limb development. Dev Biol. 2015;397(2):191-202.
56. Kawamura S, Hervold K, Ramirez-Weber FA, Kornberg TB. Two patched protein subtypes and a conserved domain of group I proteins that regulates turnover. J Biol Chem. 2008;283(45):30964-9.
57. Carpenter D, Stone DM, Brush J, Ryan A, Armanini M, Frantz G, et al. Characterization of two patched receptors for the vertebrate hedgehog protein family. Proc Natl Acad Sci U S A. 1998;95(23):13630-4.
58. Karagoz Z, Geuens T, LaPointe VLS, van Griensven M, Carlier A. Win, Lose, or Tie: Mathematical Modeling of Ligand Competition at the Cell-Extracellular Matrix Interface. Front Bioeng Biotechnol. 2021;9:657244.
59. Pathi S, Pagan-Westphal S, Baker DP, Garber EA, Rayhorn P, Bumcrot D, et al. Comparative biological responses to human Sonic, Indian, and Desert hedgehog. Mech Dev. 2001;106(1-2):107-17.
60. Kumar V, Vashishta M, Kong L, Wu X, Lu JJ, Guha C, et al. The Role of Notch, Hedgehog, and Wnt Signaling Pathways in the Resistance of Tumors to Anticancer Therapies. Front Cell Dev Biol. 2021;9:650772.
61. Carballo GB, Honorato JR, de Lopes GPF, Spohr T. A highlight on Sonic hedgehog pathway. Cell Commun Signal. 2018;16(1):11.
62. Beachy PA, Hymowitz SG, Lazarus RA, Leahy DJ, Siebold C. Interactions between Hedgehog proteins and their binding partners come into view. Genes Dev. 2010;24(18):2001-12.
63. Szalkowski AM, Anisimova M. Graph-based modeling of tandem repeats improves global multiple sequence alignment. Nucleic Acids Res. 2013;41(17):e162.
64. Boch J, Scholze H, Schornack S, Landgraf A, Hahn S, Kay S, et al. Breaking the code of DNA binding specificity of TAL-type III effectors. Science. 2009;326(5959):1509-12.
65. Mak AN, Bradley P, Bogdanove AJ, Stoddard BL. TAL effectors: function, structure, engineering and applications. Curr Opin Struct Biol. 2013;23(1):93-9.
66. Bishoy Wadie VK, Elissavet Sandaltzopoulou, Caroline Benz, Evangelia Petsalaki. Use of viral motif mimicry improves the proteome-wide discovery of human linear motifs. bioRxiv. 2021.
67. Davey NE, Cyert MS, Moses AM. Short linear motifs - ex nihilo evolution of protein regulation. Cell Commun Signal. 2015;13:43.
68. Yoshiie K, Kim HY, Mott J, Rikihisa Y. Intracellular infection by the human granulocytic ehrlichiosis agent inhibits human neutrophil apoptosis. InfectImmun. 2000;68(3):1125-33.

69. Balcewicz-Sablinska MK, Keane J, Kornfeld H, Remold HG. Pathogenic Mycobacterium tuberculosis evades apoptosis of host macrophages by release of TNF-R2, resulting in inactivation of TNF-alpha. Journal of immunology. 1998;161(5):2636-41.
70. Sly LM, Hingley-Wilson SM, Reiner NE, McMaster WR. Survival of Mycobacterium tuberculosis in host macrophages involves resistance to apoptosis dependent upon induction of antiapoptotic Bcl-2 family member Mcl-1. Journal of immunology. 2003;170(1):430-7.
71. Clifton DR, Goss RA, Sahni SK, van Antwerp D, Baggs RB, Marder VJ, et al. NF-kappa B-dependent inhibition of apoptosis is essential for host cellsurvival during Rickettsia rickettsii infection. Proceedings of the National Academy of Sciences of the United States of America. 1998;95(8):4646-51.
72. Fan T, Lu H, Hu H, Shi L, McClarty GA, Nance DM, et al. Inhibition of apoptosis in chlamydia-infected cells: blockade of mitochondrial cytochrome c release and caspase activation. The Journal of experimental medicine. 1998;187(4):487-96.
73. Bergsbaken T, Cookson BT. Macrophage activation redirects yersinia-infected host cell death from apoptosis to caspase-1-dependent pyroptosis. PLoS pathogens. 2007;3(11):e161.
74. Liu H, Bao W, Lin M, Niu H, Rikihisa Y. Ehrlichia type IV secretion effector ECH0825 is translocated to mitochondria and curbs ROS and apoptosis by upregulating host MnSOD. Cell Microbiol. 2012;14(7):1037-50.
75. Voth DE, Broederdorf LJ, Graham JG. Bacterial Type IV secretion systems: versatile virulence machines. Future Microbiol. 2012;7(2):241-57.
76. Mogga SJ, Mustafa T, Sviland L, Nilsen R. Increased Bcl-2 and reduced Bax expression in infected macrophages in slowly progressive primary murine Mycobacterium tuberculosis infection. Scand J Immunol. 2002;56(4):383-91.
77. Poirier V, Bach H, Av-Gay Y. Mycobacterium tuberculosis promotes anti-apoptotic activity of the macrophage by PtpA protein-dependent dephosphorylation of host GSK3alpha. J Biol Chem. 2014;289(42):29376-85.
78. Trnski D, Sabol M, Gojevic A, Martinic M, Ozretic P, Musani V, et al. GSK3beta and Gli3 play a role in activation of Hedgehog-Gli pathway in human colon cancer - Targeting GSK3beta downregulates the signaling pathway and reduces cell proliferation. Biochim Biophys Acta. 2015;1852(12):2574-84.
79. Stecca B, Ruiz i Altaba A. A GLI1-p53 inhibitory loop controls neural stem cell and tumour cell numbers. The EMBO journal. 2009;28(6):663-76.
80. Sheng W, Dong M, Zhou J, Li X, Liu Q, Dong Q, et al. The clinicopathological significance and relationship of Gli1, MDM2 and p53 expression in resectable pancreatic cancer. Histopathology. 2014;64(4):523-35.
81. Kuriakose JA, Miyashiro S, Luo T, Zhu B, McBride JW. Ehrlichia chaffeensis transcriptome in mammalian and arthropod hosts reveals differential gene expression and post transcriptional regulation. PLoS One. 2011;6(9):e24136.
82. McBride JW, Ndip LM, Popov VL, Walker DH. Identification and functional analysis of an immunoreactive DsbA-like thio-disulfide oxidoreductase of Ehrlichia spp. Infect Immun. 2002;70(5):2700-3.
83. Luo T, Zhang X, McBride JW. Major species-specific antibody epitopes of the Ehrlichia chaffeensis p120 and E. canis p140 orthologs in surface-exposed tandem repeat regions. Clin Vaccine Immunol. 2009;16(7):982-90.

84. Luo T, McBride JW. *Ehrlichia chaffeensis* TRP32 interacts with host cell targets that influence intracellular survival. Infect Immun. 2012;80(7):2297-306.
85. Luo T, Dunphy PS, McBride JW. Ehrlichia chaffeensis Tandem Repeat Effector Targets Differentially Influence Infection. Front Cell Infect Microbiol. 2017;7:178.
86. Mitra S, Dunphy PS, Das S, Zhu B, Luo T, McBride JW. Ehrlichia chaffeensis TRP120 Effector Targets and Recruits Host Polycomb Group Proteins for Degradation To Promote Intracellular Infection. Infect Immun. 2018;86(4).
87. Li Q, Lau A, Morris TJ, Guo L, Fordyce CB, Stanley EF. A syntaxin 1, Galpha(o), and N-type calcium channel complex at a presynaptic nerve terminal: analysis by quantitative immunocolocalization. J Neurosci. 2004;24(16):4070-81.
88. Burgess A, Vigneron S, Brioudes E, Labbe JC, Lorca T, Castro A. Loss of human Greatwall results in G2 arrest and multiple mitotic defects due to deregulation of the cyclin B-Cdc2/PP2A balance. Proceedings of the National Academy of Sciences of the United States of America. 2010;107(28):12564-9.
89. Liu W, Xie Y, Ma J, Luo X, Nie P, Zuo Z, et al. IBS: an illustrator for the presentation and visualization of biological sequences. Bioinformatics. 2015;31(20):3359-61.

Figure Legends

Fig. 1. TRP120 TR motif shares sequence and functional similarity with Hh ligands.

(A) Schematic representation of TRP120 showing domain organization. TRP120 consists of a N-terminal (NT), C-terminal (CT) and tandem repeat (TR1 – 4; 80 aa each) domain, flanked with two partial repeats (PR) (89). NCBI Protein BLAST identified an 8 amino acid short linear motif (SLiM) of high similarity between the TRP120 TR and Hh ligand amino acid sequences corresponding to the location of Hh ligand and Hh PTCH receptor-binding site (37, 62). Complete amino acid sequence of one TR is shown with homologous Hh SLiM identified in blue. Blue shaded TR regions shown in schematic indicate location of Hh SLiM. Table summarizes amino acid sequence similarity between Hh ligands and TRP120; (B-D) ISM analysis of TRP120 and Dhh/Ihh; (B) Cross-spectrum of TRP120 (accession no. AAO12927.1) and Dhh (NP_066382) with ISM frequencies (x axis) plotted against normalized amplitude for each component (y axis); (C) Cross-spectrum of TRP120 and Ihh (NP_002172) with ISM frequencies (x axis) plotted against normalized amplitude for each component (y axis); (D) Scanning of the amino acid sequence of Dhh/Ihh along ISM F[0.457] immediately upstream of the TRP120 Hh SLiM. The TRP120 TR region is defined in red.

Fig. 2. iRNA knockdown of Hh signaling components inhibits *E. chaffeensis* infection.

(A) Small interfering RNA-transfected (siRNA) THP-1 cells were infected or mock infected (-) with *E. chaffeensis* (MOI 100, 24 h post-transfection). Scrambled siRNA

(scrRNA) was transfected for positive (infected) and negative control (mock infected*). E. chaffeensis* infection was quantified at 24 hpi and was determined by qPCR amplification of the *dsb* gene. siRNA knockdown (KD) of Hh receptors PTCH2, SMO, and transcription factors GLI-1/2/3 significantly inhibits *E. chaffeensis* infection in THP-1 cells. All knockdowns were performed with at least three biological and technical replicates for *t*-test analysis. Data are represented as means ± SD (***p<0.001). (B) Western blot depicts KD efficiency of siRNA in KD cells compared to positive control from whole-cell lysates harvested 24 hpi. Number left of siRNA lane indicates percent knockdown of protein of interest relative to positive control, normalized to GAPDH expression.

Fig. 3. TRP120 interacts directly with Hh receptor PTCH2.

(A) Immunofluorescence micrographs showing the distribution of TRP120 and PTCH2 receptor in uninfected and *E. chaffeensis*-infected cells. Co-localization of *E. chaffeensis* expressing TRP120 (green) with Hh receptor PTCH2 (red) at the ehrlichial inclusion was observed at 48 hpi compared to uninfected cells. Pearson's correlation coefficient (PCC) indicates a very strong correlation between TRP120 and PTCH2, suggesting a direct interaction (scale bar, 10μm). (B) Immunofluorescence analysis of GFP tagged TRP120 transfected HeLa cells. GFP-TRP120 or GFP (ctrl) expressing HeLa cells were immunostained with PTCH2 specific antibody and observed by epifluorescence microscopy. Colocalization of GFP-tagged TRP120 (green) with the PTCH2 receptor (red) was observed in HeLa cells. (A-B) Experiments were performed with at least three biological and technical replicates. Randomized areas/slide (n=10)

were used to detect interaction. (C) Co-IP and reverse Co-IP demonstrate the direct interaction between TRP120 and PTCH2 at 24 hpi compared to the IgG negative control. Western blot analysis was normalized to GAPDH expression and experiment was repeated with three biological replicates. (D) Surface plasmon resonance (SPR) was utilized to detect the direct interaction of rPTCH2 with rTRP120-TR or rPTCH2 with rTrx (-). rPTCH2 was immobilized on a nickel chip followed by the injection of an analyte solution containing solubilized rTRP120-TR or rTrx (-) to determine the binding affinity (K_D). The binding affinity demonstrates a strong interaction between rPTCH2 and rTRP120-TR. The results were expressed as the means ± standard deviation (SD) of data obtained from three independent experiments

Fig. 4. *E. chaffeensis* activates the Hh signaling pathway in THP-1 cells and PHMs. (A) Confocal microscopy of uninfected and *E. chaffeensis* infected THP-1 cells stained with anti-GLI-1 antibody at 2, 4, 10, 24 and 48 hpi, showing a temporal increase in GLI-1 compared to the uninfected controls. Uninfected and *E. chaffeensis* infected THP-1 cells were stained with anti-DSB antibody (red) at 2, 4, 10, 24 and 48 hpi demonstrating infection of THP-1 cells with *E. chaffeensis* (scale bar = 10 μm). (B) Confocal microscopy of uninfected and *E. chaffeensis*-infected PHMs at 10 hpi showing activation of GLI-1 (green). Uninfected and *E. chaffeensis*-infected PHMs were stained with anti-DSB antibody (red) to confirm *E. chaffeensis* infection (scale bar = 10 μm). (A-B) Experiments were performed with at least three biological and technical replicates. Randomized areas/slide (n=10) were used to detect GLI-1 nuclear translocation.

Fig. 5. Expression array analysis of Hh-signaling genes during *E. chaffeensis* infection.

(A) Volcano plots showing the differential expression of Hh-signaling pathway genes between *E. chaffeensis*-infected and uninfected THP-1 cells at 4 h (top left), 8 h (top right), 24 h (bottom left) and 48 hpi (bottom right). The red, black and green dots in the volcano plot represent upregulation (≥ 2), no change, and down-regulation (≤ -2), respectively. The horizontal blue lines on the volcano plots determine the level of significance (≤ 0.05). Genes were significantly upregulated at all time points. (B) Normalized expression of Hh array genes in component, target and associated gene categories between *E. chaffeensis*-infected and uninfected cells at 48 hpi. Cells were harvested with three biological and technical replicates for all time points.

Fig. 6. *E. chaffeensis* infection alters levels of Hh-signaling components in THP-1 cells.

(A) Western blot analysis of GLI-1 levels in uninfected and *E. chaffeensis*-infected THP-1 cell nuclear fractions collected at 0, 2, 4, 10, 24 and 48 hpi with PCNA as a nuclear control. Western blot analysis of cytoplasmic fraction levels of SMO, SUFU and Shh in uninfected and *E. chaffeensis*-infected THP-1 cells at 0, 2, 4, 10, 24 and 48 hpi with GAPDH as a loading control. (B) Bar graphs depicting Western blot densitometry values were normalized to PCNA or GAPDH, respectively. (A-B) Western blots were performed with at least three biological and technical replicates for *t*-test analysis. Data are represented as means ± SD (*p<0.05).

Fig. 7. *E. chaffeensis* TRP120 activates GLI-1 and Hh gene target expression consistent with Hh ligands.

(A) Confocal immunofluorescence microscopy of untreated (-) or rTRP120-FL-, rTrx- (-), rShh-treated (+) (1 µg/mL) THP-1 cells stained with GLI-1 antibody. Micrographs demonstrate increased levels of GLI-1 (green) in rTRP120- and rShh-treated THP-1 cells 6 h post-treatment (hpt) (scale bar = 10 µm). (B) Confocal immunofluorescence microscopy of untreated, rTRP120-FL, Trx- (-) and rShh-treated (+) (1 µg/mL) PHMs harvested at 10 h. rTRP120-FL activation of GLI-1 (green) similar to rShh (positive control) in PHMs (scale bar = 10 µm). (A-B) Experiments were performed with at least three biological and technical replicates. Randomized areas/slide (n=10) were used to detect GLI-1 nuclear translocation. (C) The volcano plot is representing Hh signaling PCR array gene expression in THP-1 cells stimulated with rTRP120-FL (1 µg/mL) after normalization to control cells treated with rTrx (1 µg/mL). The respective normalized expression of rTRP120-FL regulated Hh array genes were performed with three biological and technical replicates. (D) The volcano plot is representing Hh signaling PCR array gene expression in cells stimulated with rShh (1 µg/mL) after normalized to DMSO (control) treated cell. The respective normalized expression of rShh regulated Hh array genes were performed in biological and technical replicates. (C-D) The red, black and green dots in the volcano plot represents an upregulation (≥ 2), no change and down-regulation (≤ -2), respectively for a given gene on the array. The horizontal blue lines on the volcano plots determine the level of significance ($p \leq 0.05$).

Fig. 8. TRP120 Hh SLiM activates GLI-1 in THP-1 cells and PHMs.

(A) TRP120-TR-Hh and TRP120-Hh-SLiM sequences contain the Hh homology sequence identified by BLAST analysis. TRP120-Hh-SLiM-mut contains guanine and adenine substitutions in the Hh SLiM region and is used as a negative control. TRP120-TR (-) is a sequence within the TRP120-TR that does not contain the defined Hh homology sequence. (B) Confocal immunofluorescence microscopy of untreated (-) or peptide treated THP-1 cells. THP-1 cells were stained with GLI-1 antibody. The micrograph shows increased levels of GLI-1 (green) in TRP120-TR-Hh and TRP120-Hh-SLiM treated, but not untreated, TRP120-TR (-) or TRP120-Hh-SLiM-mut treated THP-1 cells 6 h post-treatment (hpt) (scale bar = 10 μm). (C) Confocal immunofluorescence microscopy of untreated or SLiM/SLiM mutant peptide treated PHMs harvested at 10 h. The TRP120-Hh-SLiM sequence activates GLI-1 (green) in PHMs, but the corresponding mutant sequence does not (scale bar = 10 μm). (B-C) Experiments were performed with at least three biological and technical replicates. Randomized areas/slide (n=10) were used to detect GLI-1 nuclear translocation. (D-E) Hh signaling PCR arrays were utilized to analyze the expression of 84 Hh genes during infection. In brief, THP-1 cells were treated with TRP120-Hh-SLiM or TRP120-Hh-SLiM-mut (50 and 500 ng/mL) or left untreated (negative control). THP-1 cells were harvested at 6 h with three biological and technical replicates. The tables represent the fold change in gene expression at each concentration. (D) The upregulation of gene expression in TRP120-Hh-SLiM-treated cells compared to untreated cells at respective concentrations. (E) Upregulation of gene expression in TRP120-Hh-SLiM treated cells compared to TRP120-Hh-SLiM-mut treated cells at respective concentrations.

Fig. 9. Anti-TRP120 Hh SLiM antibody blocks Hh signaling and GLI-1 nuclear translocation.

(A) *E. chaffeensis* (MOI 100) and SLiMs were incubated with α-TRP120-I1 (targets TRP120 sequence SKVEQEETNPEVLIKDLQDVAS) or α-TRP32 (neg ctrl) (1.5 μg/mL) for 1 h before incubation with THP-1 cells. THP-1 cells were harvested at 10 hpt, immunostained with GLI-1 (green), and visualized by confocal fluorescence microscopy. Scale bar = 10 μm. 10 randomized areas/slide were used to detect GLI-1 nuclear translocation. (B) Western blot analysis of treatment groups with GAPDH as a loading control. Data are represented as means ± SD (*p<0.05). (A-B); α-TRP120-I1 inhibits GLI-1 activation in cells with *E. chaffeensis* or TRP120-Hh-SLiM compared to α-TRP32. Untreated cells were incubated with α-TRP120-I1 or α-TRP32 as negative controls. Experiments were performed with at least three biological and technical replicates and significance was determined through *t*-test analysis. Randomized areas/slide (n=10) were used to detect GLI-1 nuclear translocation.

Fig. 10. *E. chaffeensis* deploys the TRP120 Hh SLiM to induce BCL-2 expression for survival.

(A) Western blot analysis of BCL-2 levels of *E. chaffeensis* infected THP-1 cells collected at 0, 24, 48 and 72 hpi with GAPDH as a loading control and DSB as an infection control. *E. chaffeensis* induces BCL-2 protein expression. (B) BCL-2 levels of TRP120-Hh-SLiM and TRP120-Hh-SLiM-mut treated and untreated THP-1 cells collected at 12 hpt with GAPDH as a loading control. The TRP120-Hh-SLiM peptide induces BCL-2 protein expression, but the mutant does not. (B, C) Bar graphs depict

Western blot densitometry values normalized to GAPDH**.** (C) siRNA knockdown (KD) of BCL-2 significantly reduces *E. chaffeensis* infection in THP-1 cells as determined by qPCR amplification of the *dsb* gene. Scrambled siRNA (scrRNA) was transfected for positive (infected) and negative control (mock infected). Western blot depicts KD efficacy of siRNA in KD cells compared to the positive control. Number left of siRNA lane indicates percent KD of BCL-2 relative to positive control, normalized to GAPDH expression. (A-C) Experiments were performed with at least three biological and technical replicates and significance was determined through *t*-test analysis. Data are represented as means ± SD (*p< 0.05; **p< 0.01; ***p< 0.001)

Fig. 11. *E. chaffeensis* mediated activation of Hh signaling inhibits host cell apoptosis.

(A) Immunofluorescence analysis of uninfected and *E. chaffeensis*-infected THP-1 cells stained with JC-1 dye after treatment with 100 µM of Etoposide or DMSO control. The micrographs demonstrate the formation of JC aggregates (orange; 590±17.5 nm) in mitochondria with positive membrane potential in DMSO treated cells (top panel). Due to depolarization of the mitochondrial membrane in Etoposide-treated cells, JC-1 remains as a monomer and yields green fluorescence with the emission of 530±15 nm (middle). *E. chaffeensis*-infected Etoposide-treated THP1 cells showed increased cells with JC-1 aggregates, indicating active inhibition of host cell apoptosis during *E. chaffeensis* infection (bottom). (B) Bar graph depicts % normal or apoptotic cells in DMSO, Etoposide or Etoposide + *E. chaffeensis* groups. There were significantly fewer apoptotic cells in DMSO and Etoposide + *E. chaffeensis* groups, but significantly more

apoptotic cells in Etoposide treated groups. Experiments were performed in biological and technical replicates and significance was determined through *t*-test analysis. Data are represented as means ± SD (**p*<0.05). (C) Immunofluorescence analysis of mitochondrial membrane potential using JC-1 dye in *E. chaffeensis*-infected cells treated with Hh inhibitor Vismodegib or DMSO. The micrograph demonstrated the presence of mitochondria with positive membrane potential in DMSO treated infected cells compared to Vismodegib-treated infected cells. Arrow points to the ehrlichial inclusion. (D) Immunofluorescence analysis of uninfected and *E. chaffeensis*-infected THP-1 cells stained with Nucview488 and the Mitoview633 Dye after treatment with Vismodegib or DMSO control. The micrographs show Nucview488 dye is cleaved by caspase 3 and produces green fluorescence in Vsmodegib-treated *E. chaffeensis*-infected cells due to the activation of apoptosis. In comparison, due to positive mitochondrial membrane potential, Mitoview633 accumulated in the inner mitochondrial membrane (red) in Vismodegib-uninfected and DMSO treated (Ctrl) uninfected and infected cells. These results demonstrate that Hh signaling plays a crucial role during *E. chaffeensis* infection by inhibiting intrinsic death signaling. (A, C, D) Experiments were performed with at least three biological and technical replicates. Randomized areas/slide (n=10) were selected to visualize the phenomenon.

Fig. 12. Apoptotic profile is induced in the presence of Hh inhibitor during *E. chaffeensis* infection.

(A) Brightfield micrographs showing effects of DMSO or Hh inhibitor Vismodegib on uninfected and *E. chaffeensis* infected cells prepared using Diff-Quick staining staining.

THP-1 cells were treated with Vismodegib or DMSO (200 nM) and infected with *E. chaffeensis* or uninfected for 24 h. Infected THP-1 cells treated with Vismodegib undergo cytoplasmic condensation (precursor to apoptosis), but other treatment groups do not (arrows point to morulae). (B) Bar graph showing fold-change in *E. chaffeensis* infection for each treatment group. Ehrlichial loads were determined using qPCR measurement of *dsb* copy and normalized with host cell *GAPDH. E. chaffeensis* infection significantly declines in the presence of Vismodegib. (C) Bar graphs showing cell viability for each treatment group. Cell viability was determined using the Cellometer Mini bright field imaging and pattern-recognition assay. Cell viability significantly declines in the presence of Vismodegib during *E. chaffeensis* infection. (D) Western blot analysis of BCL-2 levels for each group with GAPDH as a loading control. BCL-2 protein expression significantly declines during *E. chaffeensis* infection in the presence of Vismodegib. (E) Western blot analysis of pro and cleaved caspase 9 levels for each group with GAPDH as a loading control. Pro caspase 9 protein expression significantly declines while cleaved caspase 9 protein expression significantly increases during *E. chaffeensis* infection in the presence of Vismodegib. (F) Western blot analysis of pro and cleaved caspase 3 levels for each group with GAPDH as a loading control. pro caspase 3 protein expression significantly declines while cleaved caspase 3 protein expression significantly increases during *E. chaffeensis* infection in the presence of Vismodegib. (D-F) Bar graphs depict Western blot densitometry values normalized to GAPDH**.** (B-F) (A-F) Experiments were performed with at least three biological and technical replicates and significance was determined through *t*-test analysis. Data are represented as means ± SD (*p<0.05; **p<0.01; ***p<0.001).

Fig. 13. Model of *E. chaffeensis* TRP120 SLiM mimetic activation of Hh signaling, downstream GLI-1 activation and apoptosis inhibition.

When Hh signaling is off, GLI-1 is negatively regulated by SUFU, which leads to GLI-1 phosphorylation and truncation. Truncated GLI-1 (GLI^R) translocates to the nucleus, but its repressive form is unable to activate downstream gene targets. Thus, BCL-2 is not expressed, which leads to Bax release of CytC and subsequent activation of caspase cleavage and apoptosis. Therefore, *E. chaffeensis* TRP120 SLiM interacts with the PTCH2 receptor to trigger PTCH2 lysosomal degradation, thereby activating the SMO receptor to prevent SUFU from inhibiting GLI-1. Therefore, transcription factor GLI-1 (GLI^A) translocates freely to the nucleus to bind DNA and activate Hh gene targets. Further, Hh signaling upregulates activates BCL-2 to prevent apoptosis by maintaining the integrity of the mitochondrial membrane and thus prevents Bax release of cytochrome c (CytC) and involved activation of the intrinsic caspase cascade (caspase 9, Caspase 3).

Figures

Fig.1

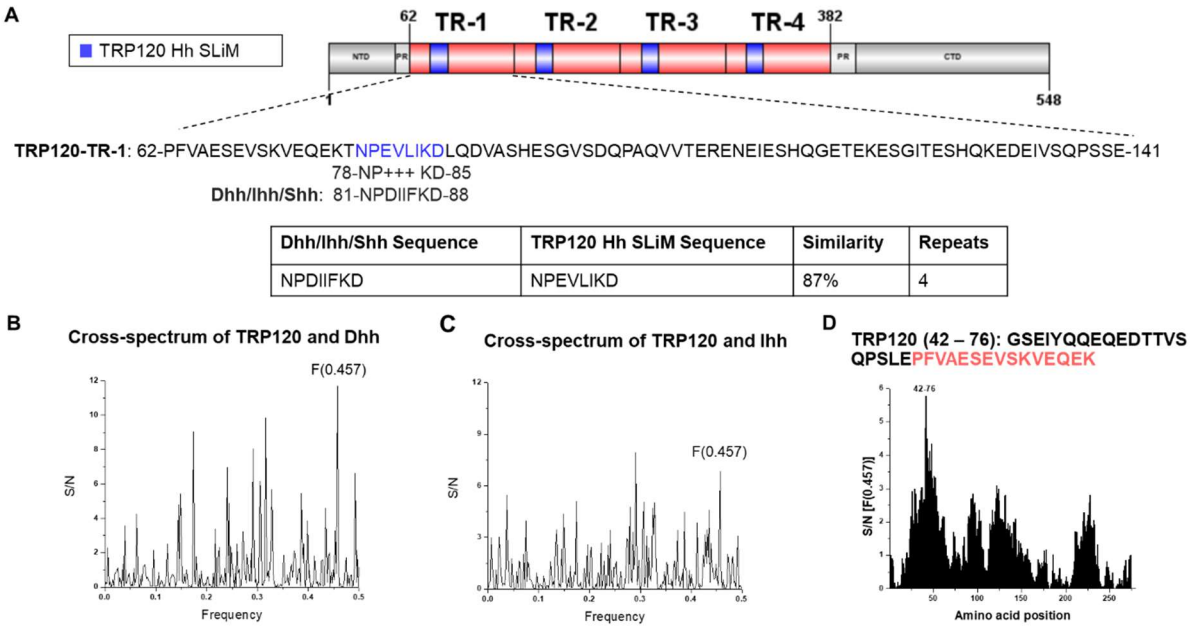

Dhh/Ihh/Shh Sequence	TRP120 Hh SLiM Sequence	Similarity	Repeats
NPDIIFKD	NPEVLIKD	87%	4

Fig. 2

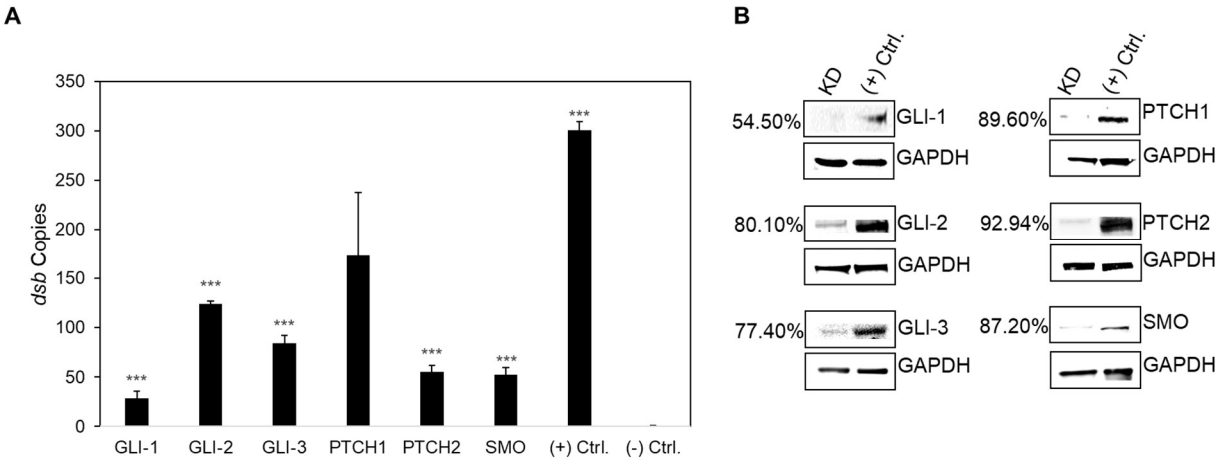

Fig. 3

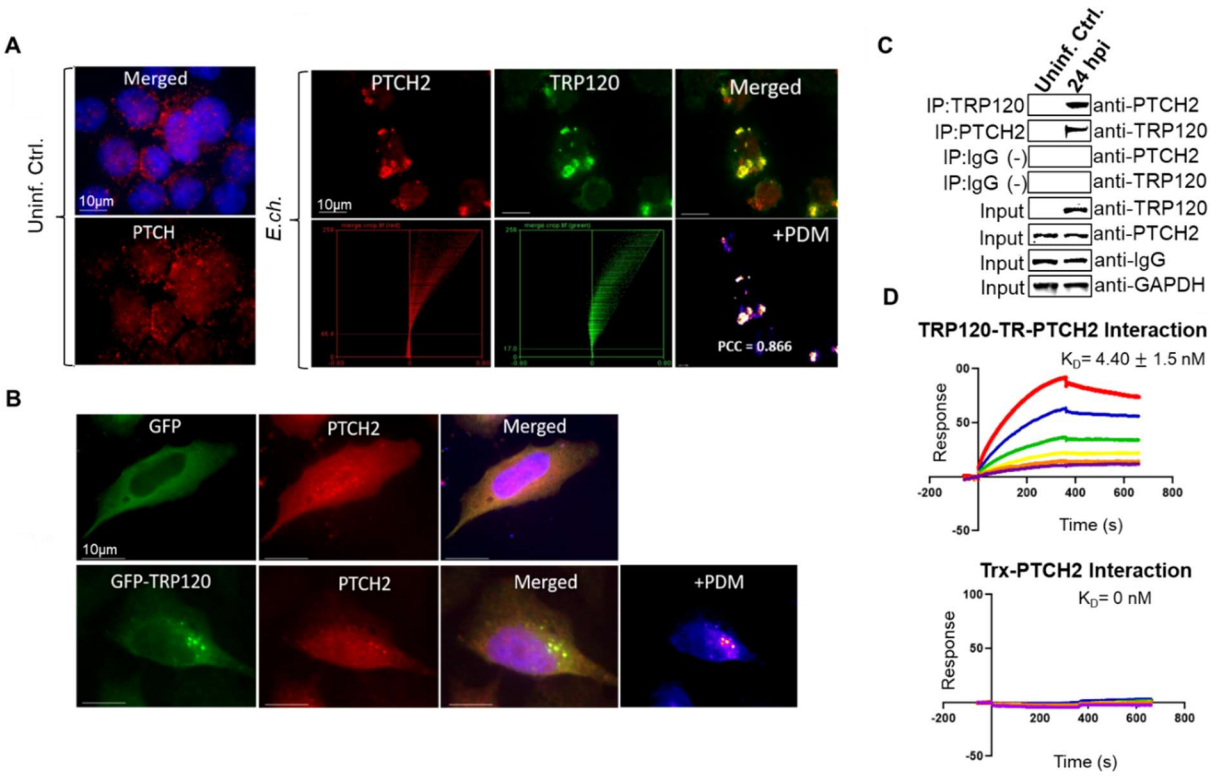

Fig. 4

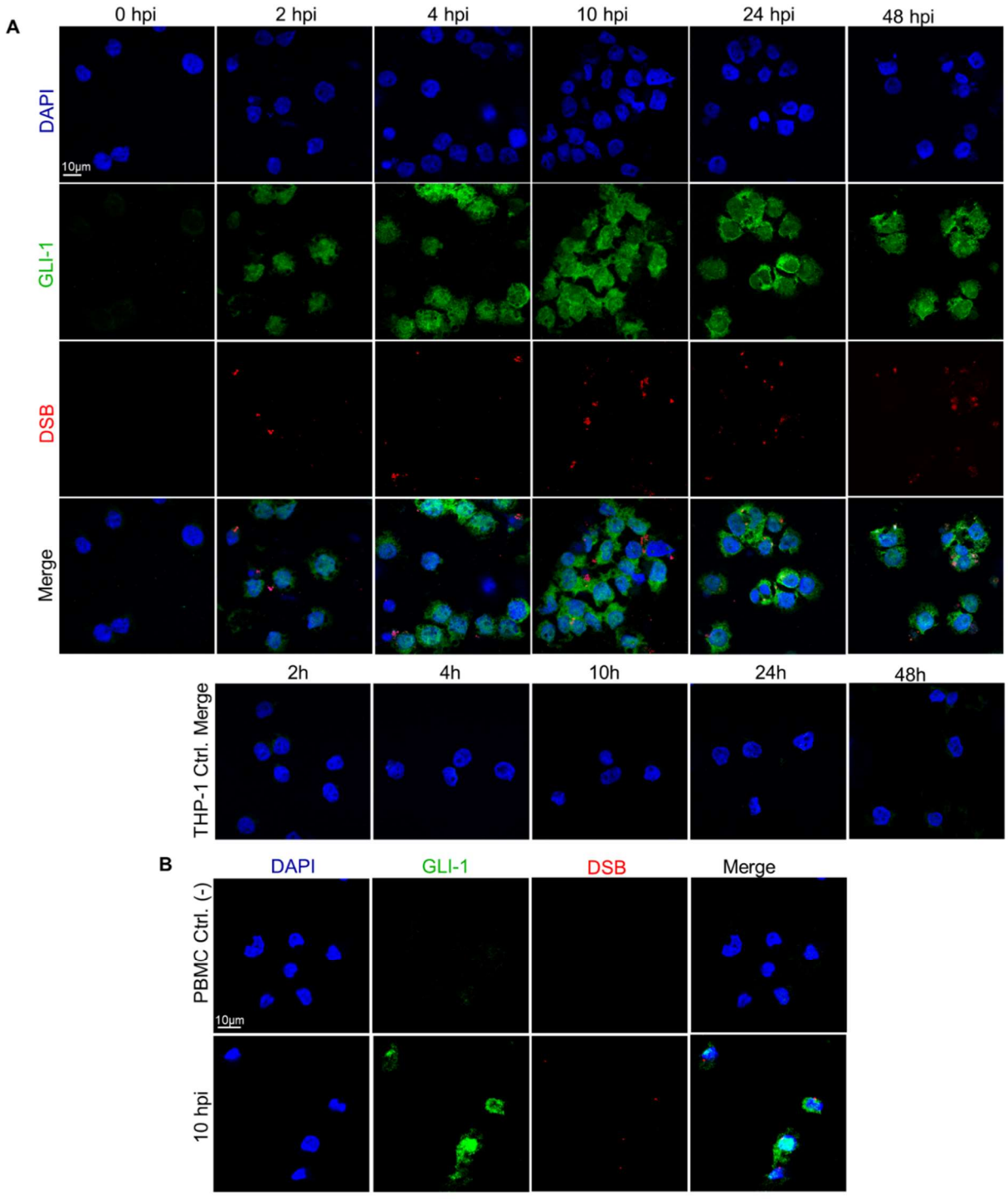

Fig. 5

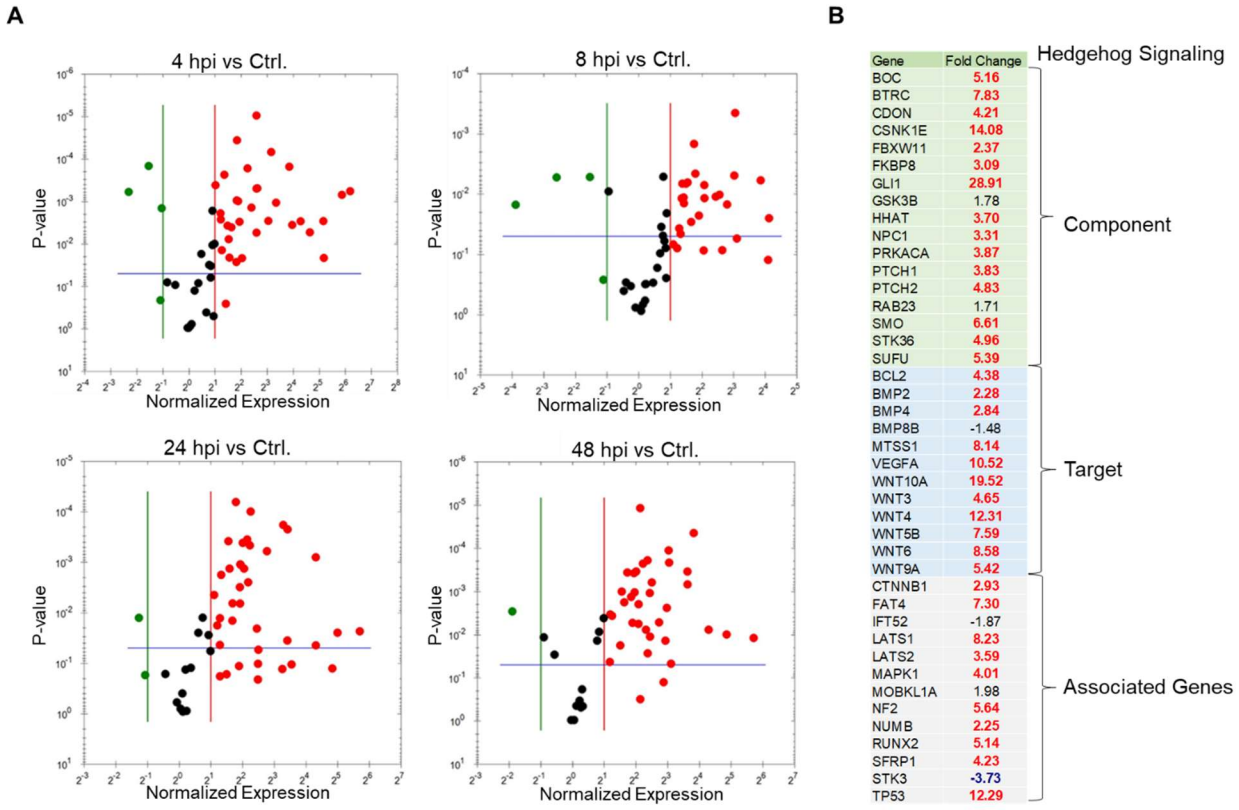

Gene	Fold Change
BOC	5.16
BTRC	7.83
CDON	4.21
CSNK1E	14.08
FBXW11	2.37
FKBP8	3.09
GLI1	28.91
GSK3B	1.78
HHAT	3.70
NPC1	3.31
PRKACA	3.87
PTCH1	3.83
PTCH2	4.83
RAB23	1.71
SMO	6.61
STK36	4.96
SUFU	5.39
BCL2	4.38
BMP2	2.28
BMP4	2.84
BMP8B	-1.48
MTSS1	8.14
VEGFA	10.52
WNT10A	19.52
WNT3	4.65
WNT4	12.31
WNT5B	7.59
WNT6	8.58
WNT9A	5.42
CTNNB1	2.93
FAT4	7.30
IFT52	-1.87
LATS1	8.23
LATS2	3.59
MAPK1	4.01
MOBKL1A	1.98
NF2	5.64
NUMB	2.25
RUNX2	5.14
SFRP1	4.23
STK3	-3.73
TP53	12.29

Fig. 6

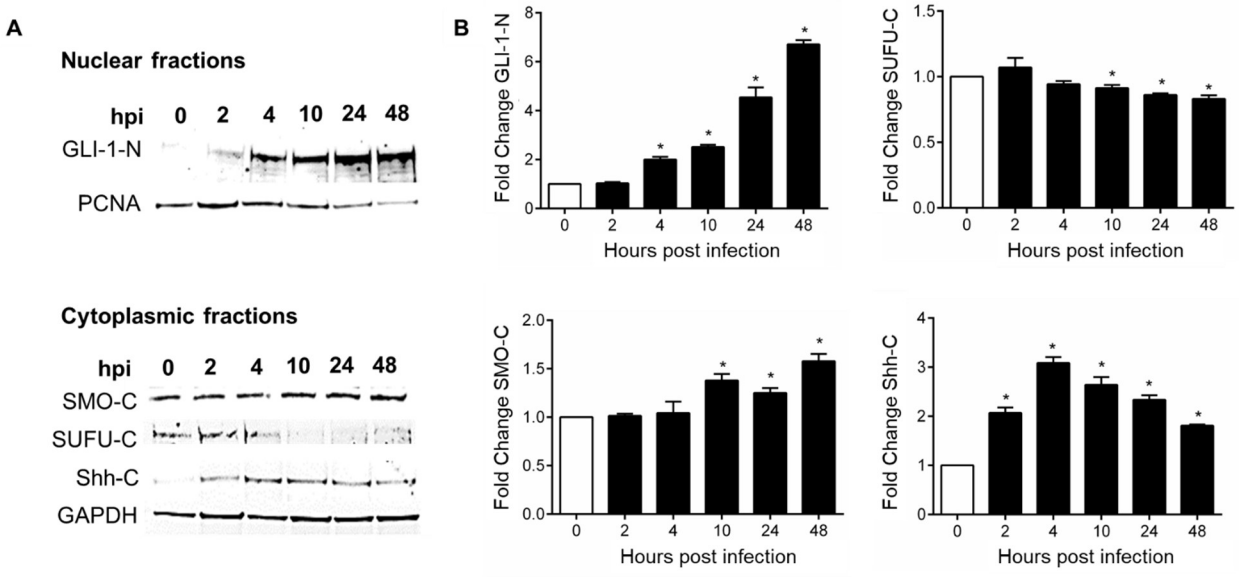

Fig. 7

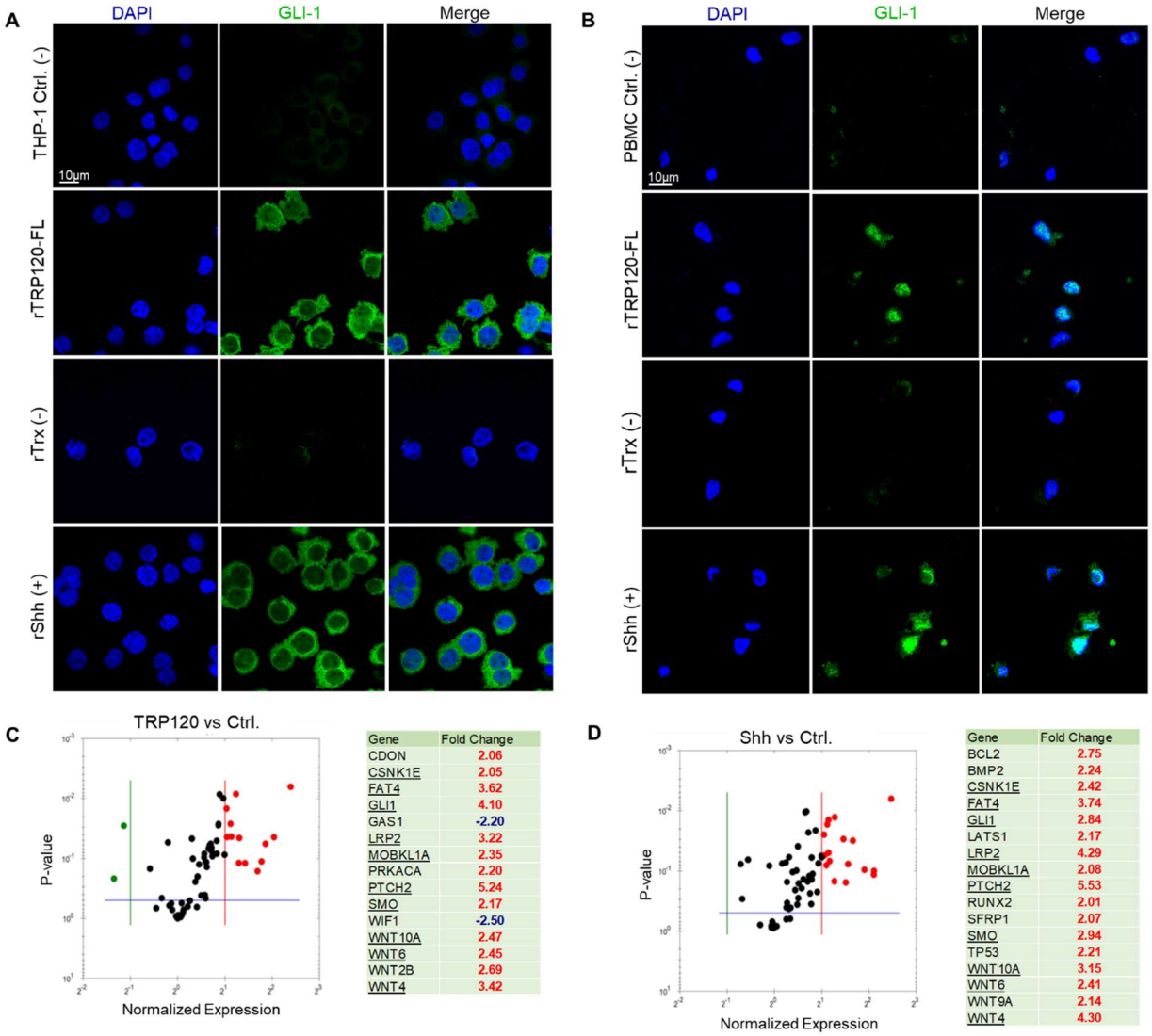

Gene	Fold Change
CDON	2.06
CSNK1E	2.05
FAT4	3.62
GLI1	4.10
GAS1	-2.20
LRP2	3.22
MOBKL1A	2.35
PRKACA	2.20
PTCH2	5.24
SMO	2.17
WIF1	-2.50
WNT10A	2.47
WNT6	2.45
WNT2B	2.69
WNT4	3.42

Gene	Fold Change
BCL2	2.75
BMP2	2.24
CSNK1E	2.42
FAT4	3.74
GLI1	2.84
LATS1	2.17
LRP2	4.29
MOBKL1A	2.08
PTCH2	5.53
RUNX2	2.01
SFRP1	2.07
SMO	2.94
TP53	2.21
WNT10A	3.15
WNT6	2.41
WNT9A	2.14
WNT4	4.30

Fig. 8

A

TRP120-TR-Hh	TRP120-TR (-)	TRP120-Hh-SLiM	TRP120-Hh-SLiM-mut
VSKVEQEKTNPEVLIKDLQD	SHQGETEKESGITESHQKEDEI	NPEVLIKD	SKVEQEKTGAGAGAGALQ

B

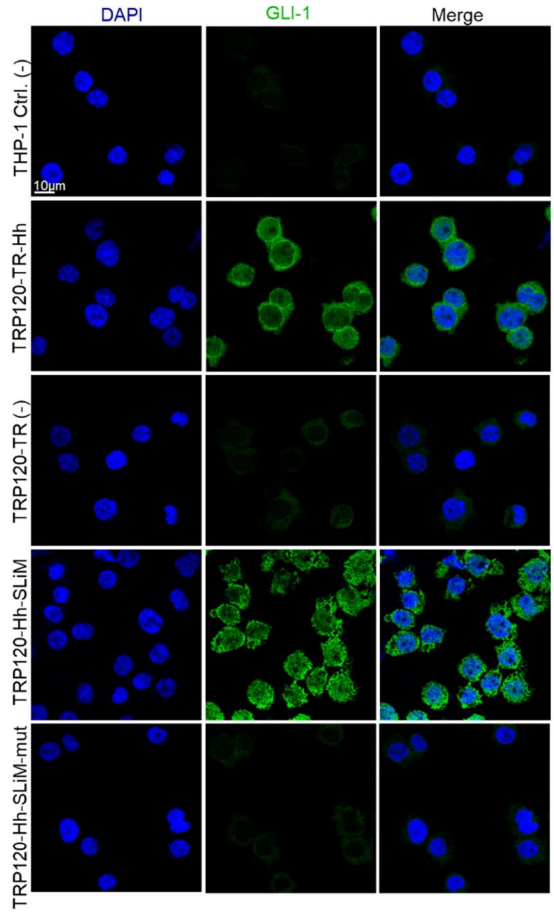

C

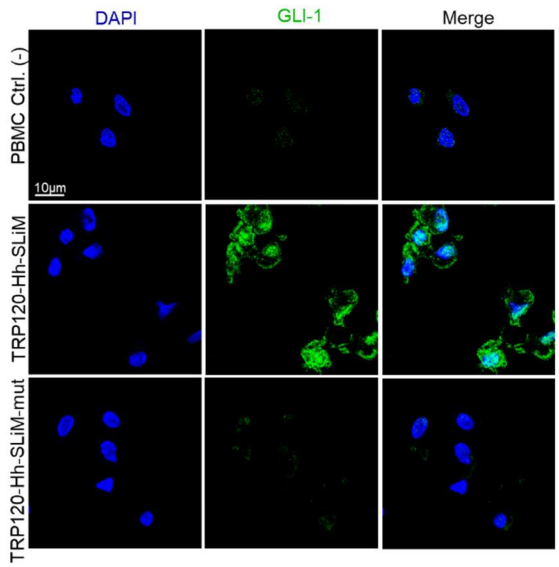

D

TRP120-Hh-SLiM vs Ctrl.		
Gene	Fold Change (50 ng/mL)	Fold Change (500 ng/mL)
BCL2	-2.39	27.79
BMP2	-1.88	26.07
BMP4	9.05	9.93
BMP6	-2.18	1059.23
BMP7	1.52	810.56
BOC	35.48	397843.88
BTRC	56.03	23241.04
CDON	38.98	17186.48
CSNK1E	12.79	99528.71
CTNNB1	-1.69	27.37
DHH	-1.66	29.54
GLI1	10.16	611054.50
GLI2	25.82	2770.58
GLI3	26.37	903.43
KCTD11	5.32	13.91
LATS1	-1.08	18.32
MAPK1	20.27	830.57
MOB1B	18.32	771.74
MTSS1	-1.27	22.37
NF2	6.45	38.41
PRKACA	9.17	2892.06
PTCH1	6.93	35.53
PTCH2	29.43	86.76
SHH	-2.56	246.41
SMO	2.54	70964.46
TP53	-5.85	64.86
VEGFA	5.40	100.17
WNT1	-16.81	138.31
WNT3	-1.79	352.32
WNT4	23.05	183.48
WNT5A	13.35	43.34
WNT5B	-2.61	13.35
WNT6	1.02	12.52
WNT9	44.76	121703.34
WNT10A	45.72	525897.87

E

TRP120-Hh-SLiM vs TRP120-Hh-SLiM-mut		
Gene	Fold Change (50 ng/mL)	Fold Change (500 ng/mL)
BCL2	-2.51	18.58
BMP2	0.45	19.72
BMP4	3.23	10.80
BMP6	0.01	1040.90
BMP7	0.02	910.34
BOC	14.12	7169.57
BTRC	9.49	4373.88
CDON	18.33	1262.45
CSNK1E	13.44	1214.72
CTNNB1	1.89	20.97
DHH	2.09	19.84
GLI1	9.78	2338.31
GLI2	38.13	1231.86
GLI3	10.14	1751.28
KCTD11	8.22	18.25
LATS1	1.33	493.20
MAPK1	6.20	1181.52
MOB1B	24.49	6318.25
MTSS1	-4.59	22.24
NF2	8.46	58.57
PRKACA	9.99	2335.09
PTCH1	15.35	52.29
PTCH2	49.35	73.41
SHH	12.52	1780.84
SMO	10.09	1524.56
TP53	0.11	56.07
VEGFA	9.38	99.18
WNT1	19.63	296.39
WNT3	2.61	1238.21
WNT4	16.47	50.86
WNT5A	3.50	49.94
WNT5B	5.15	24.00
WNT6	2.83	5.19
WNT9	32.86	39125.80
WNT10A	9.65	469.52

Fig. 9

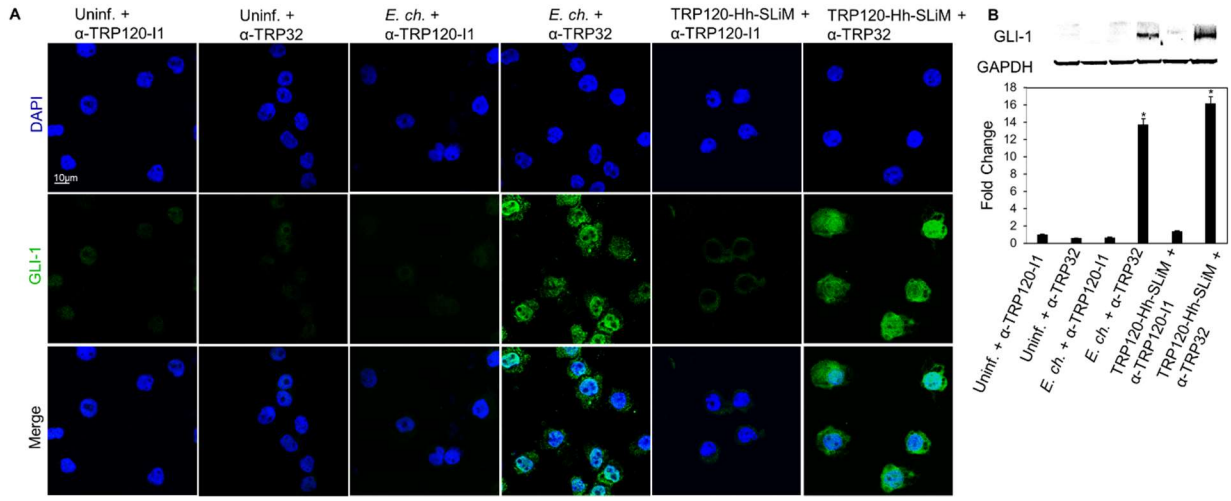

Fig. 10

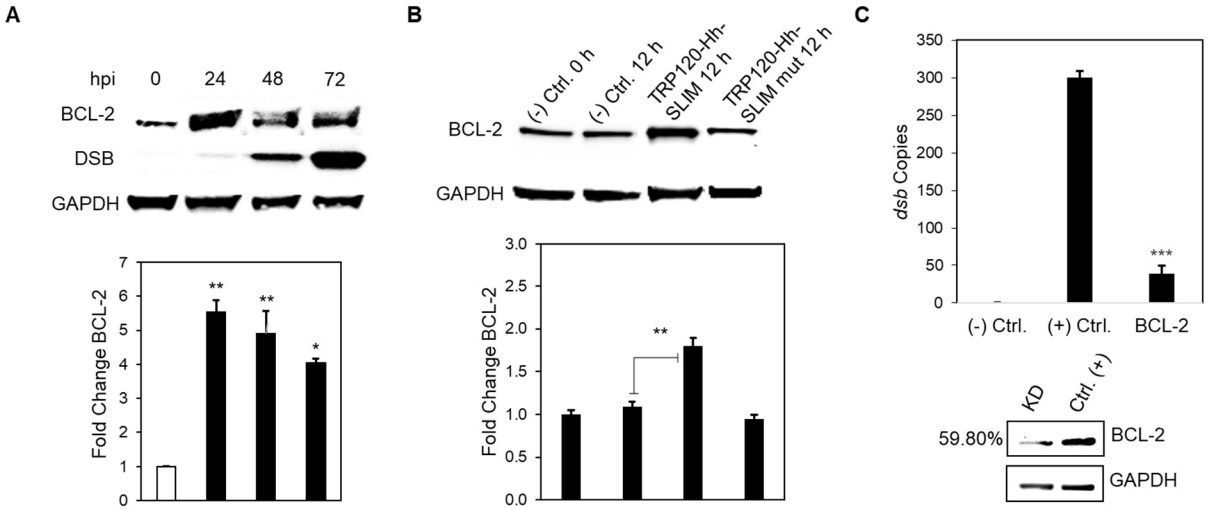

Fig. 11

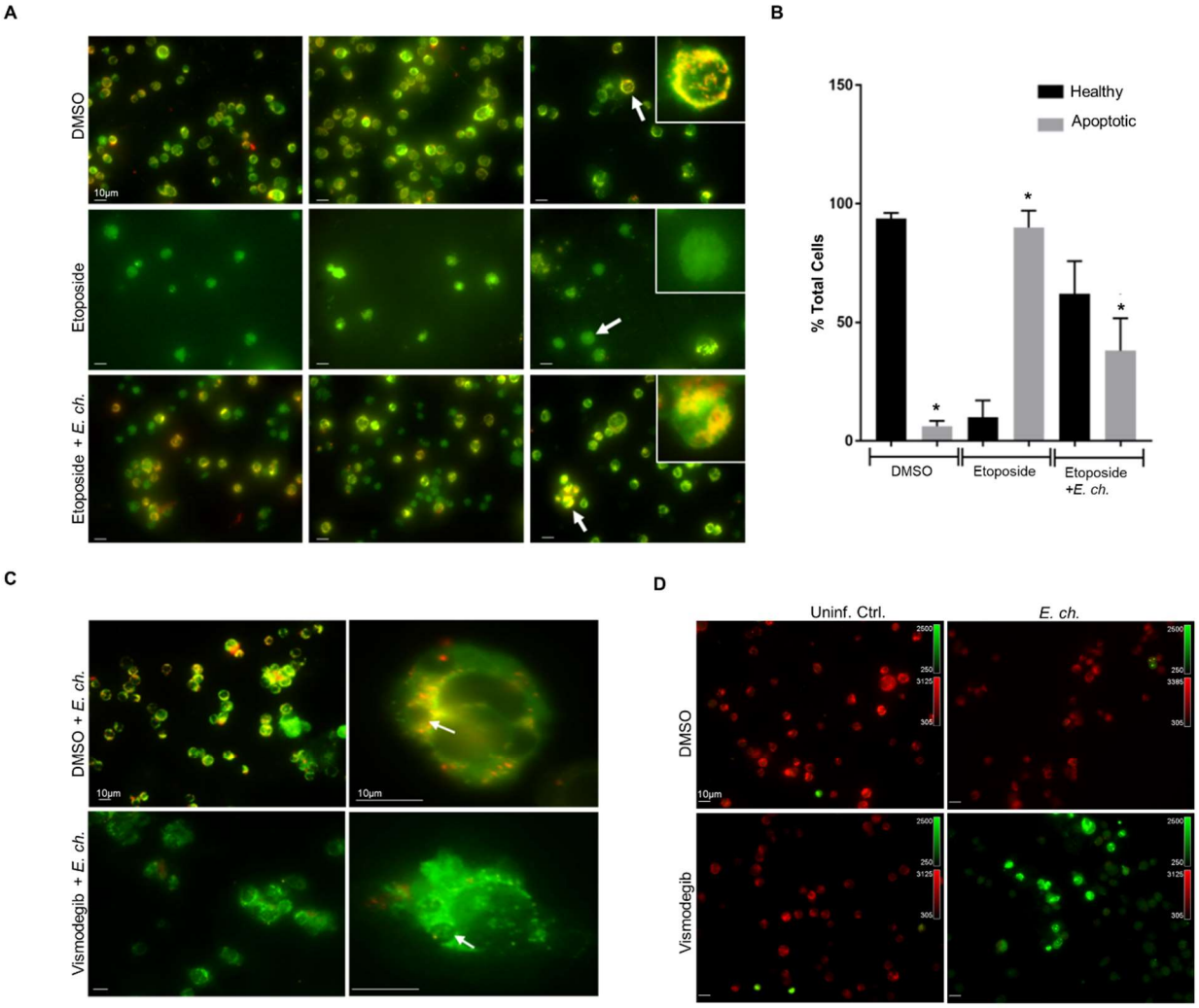

Fig. 12

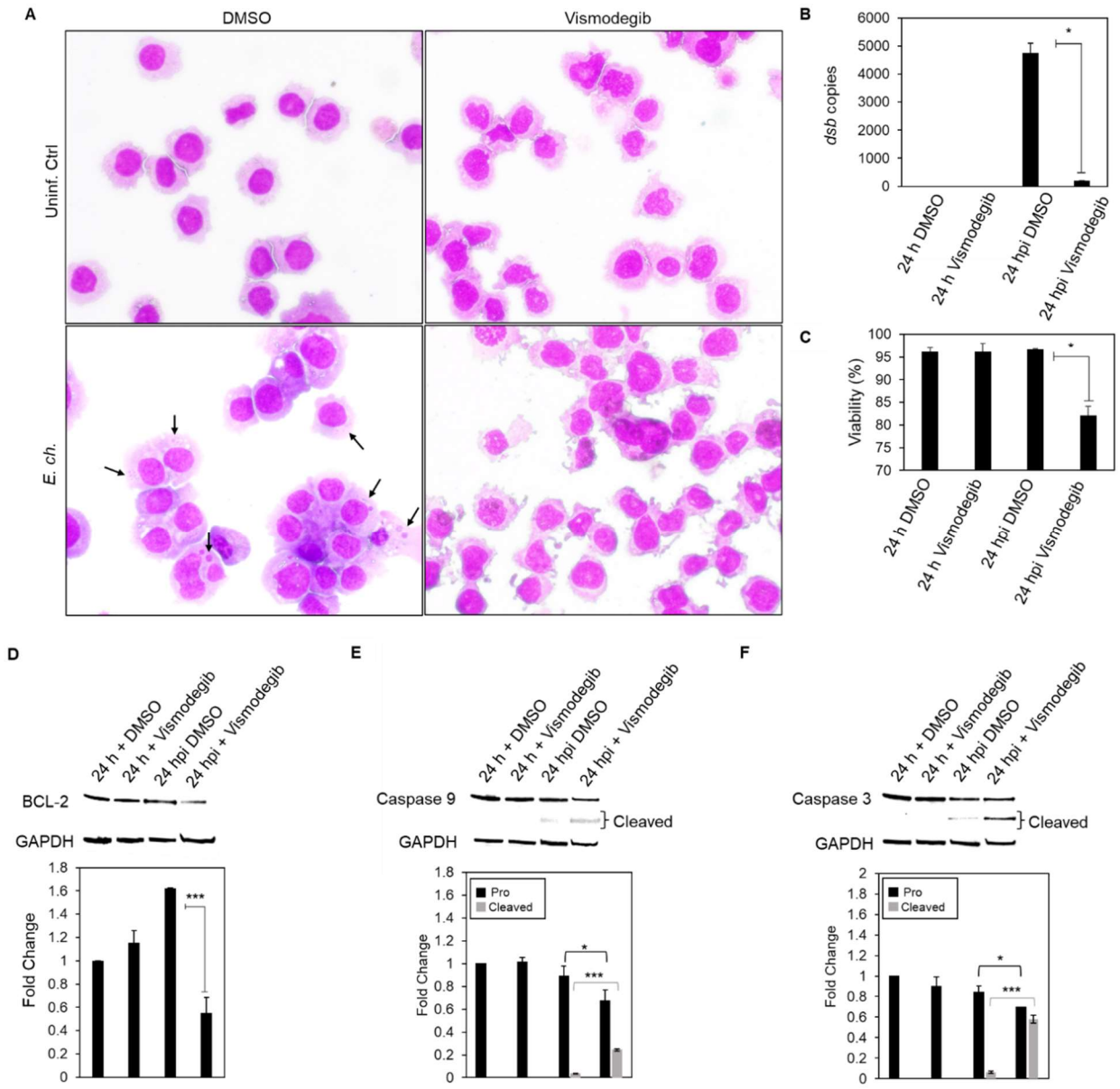

Fig. 13